TURUN YLIOPISTON JULKAISUJA
ANNALES UNIVERSITATIS TURKUENSIS

SARJA - SER. D OSA - TOM. 1006

MEDICA - ODONTOLOGICA

IN VIVO IMAGING OF VASCULAR ADHESION PROTEIN-1

Preclinical Studies with Positron Emission Tomography

by

Anu Autio

TURUN YLIOPISTO
UNIVERSITY OF TURKU
Turku 2012

From Department of Clinical Physiology and Nuclear Medicine, Turku PET Centre, MediCity Research Laboratory and Department of Medical Microbiology and Immunology and the FinPharma Doctoral Program Drug Discovery Section, University of Turku, Finland

Supervised by:

Professor Anne Roivainen, PhD
Turku PET Centre
Turku Center for Disease Modeling
University of Turku
Turku, Finland

and

Professor Sirpa Jalkanen, MD, PhD
MediCity Research Laboratory
University of Turku
Turku, Finland

Reviewed by:

Anu Airaksinen, PhD
Laboratory of Radiochemistry
University of Helsinki
Helsinki, Finland

and

Aapo Ahonen, MD, PhD
Department of Clinical Physiology and Nuclear Medicine
University Hospital of Helsinki
Helsinki, Finland

Dissertation opponent:

Professor Helmut Mäcke, MD, PhD
Department of Nuclear Medicine
University Medical Center Freiburg
Freiburg, Germany

ISBN 978-951-29-4928-1 (PRINT)
ISBN 978-951-29-4929-8 (PDF)
ISSN 0355-9483
Painosalama Oy – Turku, Finland 2012

to my family

ABSTRACT

Anu Autio

***In vivo* imaging of vascular adhesion protein 1 - preclinical studies with positron emission tomography**

Turku PET Centre, Turku University Hospital and Institute of Clinical Medicine, Department of Clinical Physiology and Nuclear Medicine, University of Turku, Turku, Finland

The golden standard in nuclear medicine imaging of inflammation is the use of radiolabeled leukocytes. Although their diagnostic accuracy is good, the preparation of the leukocytes is both laborious and potentially hazardous for laboratory personnel. Molecules involved in leukocyte migration could serve as targets for the development of inflammation imaging agents. An excellent target would be a molecule that is absent or expressed at low level in normal tissues, but is induced or up-regulated at the site of inflammation. Vascular adhesion protein-1 (VAP-1) is a very promising target for *in vivo* imaging, since it is translocated to the endothelial cell surface when inflammation occurs. VAP-1 functions as an endothelial adhesion molecule that participates in leukocyte recruitment to inflamed tissues. Besides being an adhesion molecule, VAP-1 also has enzymatic activity.

In this thesis, the targeting of VAP-1 was studied by using Gallium-68 (^{68}Ga) labeled peptides and an Iodine-124 (^{124}I) labeled antibody. The peptides were designed based on molecular modelling and phage display library searches. The new imaging agents were preclinically tested *in vitro,* as well as *in vivo* in animal models. The most promising imaging agent appeared to be a peptide belonging to the VAP-1 leukocyte ligand, Siglec-9 peptide. The ^{68}Ga-labeled Siglec-9 peptide was able to detect VAP-1 positive vasculature in rodent models of sterile skin inflammation and melanoma by positron emission tomography. In addition to peptides, the ^{124}I-labeled antibody showed VAP-1 specific binding both *in vitro* and *in vivo.* However, the estimated human radiation dose was rather high, and thus further preclinical studies in disease models are needed to clarify the value of this imaging agent.

Detection of VAP-1 on endothelium was demonstrated in these studies and this imaging approach could be used in the diagnosis of inflammatory conditions as well as melanoma. These studies provide a proof-of-concept for PET imaging of VAP-1 and further studies are warranted.

Keywords: inflammation, *in vivo* imaging, positron emission tomography (PET), vascular adhesion protein-1 (VAP-1)

TIIVISTELMÄ

Anu Autio

Verisuonten endoteelisolujen pinnalla ilmenevän tartuntamolekyylin (VAP-1) *in vivo* kuvantaminen – prekliinisiä tutkimuksia positroniemissiotomografialla

Valtakunnallinen PET-keskus, Turun yliopistollinen keskussairaala ja Kliininen laitos, Kliininen fysiologia ja isotooppilääketiede, Turun yliopisto, Turku

Vakioitu menetelmä tulehduksen lääketieteellisessä isotooppikuvantamisessa on radioleimattuja valkosolujen käyttö. Vaikka radioleimattujen valkosolujen tulehduksen kuvantamistarkkuus on hyvä, niiden valmistaminen on työlästä ja mahdollisesti vaarallista laboratoriohenkilökunnalle. Ainakin teoriassa, tulehduksessa lisääntyviä adheesiomolekyylejä voitaisiin käyttää tulehduksen *in vivo* kuvantamisen kohteina. Hyvä kohdemolekyyli on sellainen, jota ei normaalisti esiinny kudoksissa ollenkaan tai esiintyy ainoastaan hyvin vähäisissä määrissä, mutta runsaasti tulehdusalueella. Verisuonten endoteelisolujen pinnalla ilmenevä tartuntamolekyyli, VAP-1, on lupaava kohdemolekyyli tulehduksen *in vivo* kuvantamiseksi. Tulehdussignaalin seurauksena VAP-1 siirtyy endoteelisolun sisältä pintaan ja ohjaa valkosoluja verenkierrosta tulehduspaikalle.

Tässä väitöskirjatyössä VAP-1 molekyyliin kohdentuvaa kuvantamista tutkittiin käyttämällä gallium-68 (^{68}Ga) leimattuja peptidejä ja jodi-124 (^{124}I) leimattua vasta-ainetta. Peptidit suunniteltiin molekyylimallinnuksen ja yhdistelmä-DNA-tekniikalla tuotetun proteiinikirjaston avulla. Ensimmäinen tutkittu peptidi toimi VAP-1 entsyymitoiminnan inhibiittorina kun taas toinen testattu peptidi kuului VAP-1:n aikaisemmin tuntemattomalle valkosolujen vastaparille (siglec-9). Merkkiaineiden toimivuutta testattiin *in vitro* kokeilla ja *in vivo* tautimalleissa. Tutkimustulosten mukaan ^{68}Ga-leimattu Siglec-9 peptidi oli lupaavin kuvantamiseen sopiva merkkiaine. Leimattu peptidi pystyi osoittamaan VAP-1 positiivisen verisuoniston sekä melanoomassa sekä tulehdusmalleissa hiiressä ja rotassa. Peptidien lisäksi ^{124}jodi leimattu vasta-aine havaitsi VAP-1:n sekä *in vitro* että *in vivo* testeissä. ^{124}I-leimatun vasta-aineen ihmiselle arvioitu säderasitus on kuitenkin melko korkea, joten tarvitaan lisää tautimalleilla tehtäviä prekliinisiä tutkimuksia merkkiaineen käyttökelpoisuuden selvittämiseksi.

VAP-1 havaitsemista verisuonten pinnalla käytettiin näissä tutkimuksissa tulehdustilojen sekä melanooman diagnostisoimiseen. Nämä tutkimukset ovat alustavia ja merkkiaineiden käyttökelpoisuus kliinisessä ympäristössä on vielä osoitettava.

Avainsanat: positroniemissiotomografia (PET), tulehdus, *in vivo* kuvantaminen, verisuonten endoteelisolujen pinnalla ilmenevä tartuntamolekyyli (VAP-1)

TABLE OF CONTENT

ABBREVIATIONS

AUC	Area under curve
BTT-2052/ SZE5302	(1S,2S)-2-(1-methylhydrazino)-1-indanol
CL	Clearance
DOTA	1,4,7,10- tetraazacyclododecane-1,4,7-tris (t-butyl acetate)-10-acetic acid; chelator
DNCB	1-chloro-2,4-dinitrobenzene
EAE	Experimental autoimmune encephalitis
[^{18}F]-FDG	2-^{18}F-fluoro-2-deoxy-D-glucose, Glucose analogue
[^{68}Ga]-DOTAVAP-P1	DOTA-GGGGKGGGG, VAP-1 binding ^{68}Gallium labeled peptide
[^{68}Ga]-DOTAVAP-PEG-P1	DOTA-PEG-GGGGKGGGG, VAP-1 binding ^{68}Gallium labeled PEGylated peptide
GMP	Good manufacturing practice
HE	Haematoxylin and eosin staining
HEV	High endothelial venule
HPLC	High-performance liquid chromatography
HRRT	High resolution research tomograph
[^{124}I]BTT-1023	VAP-1 binding fully human antibody
IA	Injected (radio) activity
IBD	Inflammatory bowel disease
ICAM-1	Inter-cellular adhesion molecule-1
(H)IgG	(Human) Immunoglubulin G (HIG)
k_{el}	Elimination rate constant
KO	Knockout mice
KOTG	Knockout mice expressing human gene
LJP-1207	N-(2-phenyl-allyl)-hydrazine hydrochloride
LJP-1586	Z-3-fluoro-2-(4-methoxybenzyl)allylamine hydrochloride
mAbs	Monoclonal antibodies
NF-κB	Nuclear factor – κB, transcription factor

PET	Positron emission tomography
PEG	Polyethylene glycol, 8-amino-3,6-diooxaoctanoyl
PRRT	Peptide-receptor-targeted radiotherapy
PSGL1	P -selectin glycoprotein ligand-1
PSL/mm^2	Photostimulated luminescence per unit area
RA	Rheumatoid arthritis
RGD	Arginine-Glycine-Aspartic acid, amino acid sequence
RIA	Rotating radioimmunoassay
ROI	Regions of interest
SD	Standard deviation
SEM	Standard error of the mean
SUV	Standardized uptake value
SPECT	Single photon emission tomography
SSAO	Semicarbazide sensitive amine oxidase, also known as VAP-1
$t_{1/2}$	Half-life; metabolic, elimination, distribution or physical
TACs	Time-activity curves
TAMs	Tumor associated macrophages
TLC	Thin-layer chromatography
TNF-α	Tumor necrosis factor-α
TPQ	Topaquinone, co-factor
VAP-1	Vascular adhesion protein-1, also known as SSAO
VCAM-1	Vascular cell adhesion molecule-1
VOI	Volumes of interest
WBC	White blood cells
WT	Wild type mice, strain C57Black

LIST OF ORIGINAL PUBLICATIONS

This thesis is based on the following original publications, which are referred to in the text by their Roman numerals I-IV.

I. Autio A., Ujula T., Luoto P., Salomäki S., Jalkanen S., Roivainen A. (2010). PET imaging of inflammation and adenocarcinoma xenografts using vascular adhesion protein 1 targeting peptide [^{68}Ga]-DOTAVAP-P1: comparison with [^{18}F]-FDG. *Eur J Nucl Med Mol Imaging* **37**, 1918-1925.

II. Autio A., Henttinen T., Sipilä H.J., Jalkanen S., Roivainen A. (2011). Mini-PEG spacering of VAP-1-targeting [^{68}Ga]-DOTAVAP-P1 peptide improves PET imaging of inflammation. *EJNMMI Research* **1**:10.

III. Aalto K.*, Autio A.*, Kiss E.A., Elima K., Nymalm Y., Veres T.Z., Marttila-Ichihara F., Elovaara H., Saanijoki T., Crocker P.R., Maksimow M., Bligt E., Salminen T.A., Salmi M., Roivainen A., Jalkanen S. (2011). Siglec-9 is a novel leukocyte ligand for vascular adhesion protein-1 and can be used in PET imaging of inflammation and cancer. *Blood* **118**, 3725-3733. *Equal contribution

IV. Autio A, Vainio PJ, Mali A, Vainio J, Suilamo S, Oikonen V, Luoto P, Teräs M, Roivainen A. Whole-body distribution, pharmacokinetics and dosimetry of radioiodinated fully humanized anti-VAP-1 antibody – a PET imaging study of rabbits. *Manuscript submitted for publication*.

1 INTRODUCTION

In vivo imaging of inflammation is a demanding task and novel molecular imaging targets are needed. The gold standard in nuclear medicine is the radiolabelling of white blood cells. The preparation of this imaging agent is both time consuming and potentially hazardous for the technical personnel. Positron emission tomography (PET) is a powerful, non-invasive method that is particularly suitable for drug development because of its high sensitivity and ability to provide quantitative and kinetic information. PET imaging with a specific imaging agent makes it possible to investigate the presence or absence of a target molecule *in vivo*. Peptide-based imaging agents offer an interesting approach for the molecular imaging of inflammation. They are molecules that possess favorable properties, such as rapid diffusion in a target tissue, rapid clearance from the blood circulation and non-target tissues, an easy and low-cost synthesis, and low toxicity and immunogenicity. Also immuno-PET, a combination of PET with monoclonal antibodies, may provide useful quantitative information about pharmacokinetics, accumulation in targeted and non-targeted tissues, and saturation of the target antigen in patients. Both, peptides and antibodies, can be labeled in a straight forward manner with several PET isotopes, such as Gallium-68 (^{68}Ga), Copper-64 (^{64}Cu), Fluorine-18 (^{18}F), Iodine-124 (^{124}I) and Zirkonium-89 (^{89}Zr).

Imaging agents visualizing a specific progress during the development of inflammation would be valuable. Leukocyte migration from the blood into the non-lymphoid tissues is a hallmark of inflammation. Several molecules on the endothelial cell surface and their counter-receptors on vascular endothelium mediate a multistep adhesion cascade featuring tethering, rolling, activation, adhesion, crawling and transmigration phases. The vascular adhesion protein-1 (VAP-1/SSAO) is an endothelial cell molecule that is rapidly translocated from the intracellular storage granules to the endothelial cell surface upon inflammation. It contributes to several steps in the extravasation cascade and controls the trafficking of lymphocytes, granulocytes and monocytes to sites of inflammation. VAP-1 is both an optimal candidate for anti-inflammatory therapy and a potential target for the *in vivo* imaging of inflammation. Imaging agents targeting VAP-1 could be valuable, not only for the diagnosis and planning of treatment in patients, but also for the drug discovery and development processes. In addition to therapy monitoring, VAP-1 imaging would provide a tool for the basic scientist for the *in vivo* imaging of leukocyte trafficking at the sites of inflammation and cancer. In this work, I have demonstrated the possibility to image inflammation with PET by using [^{68}Ga]-labeled 1,4,7,10-tetraazacyclododecane-N',N'',N''',N''''-tetraacetic acid (DOTA) conjugated peptides and [^{124}I]-labeled antibody binding to VAP-1.

2 REVIEW OF THE LITERATURE

2.1 INFLAMMATION

When the body encounters tissue damage, it reacts to this change with inflammatory stimuli. In his review article, Medzhitov divides the causes of tissue damage to exogenous and endogenous factors (Medzhitov 2008). Exogenous factors can be further divided into microbial, such as bacteria, viruses and parasites and non-microbial, such as allergens, foreign bodies and chemical and physical irritants. Endogenous signals, such as tissue stress and malfunction are more delicate and do not cause extreme symptoms, such as tissue damage. These changes are referred to by Medzhitov as para-inflammation, at one end near the basal state and at the extreme end this phenomenon might play a role in many inflammatory diseases, such as obesity, type 2 diabetes, atherosclerosis, asthma and neurodegenerative diseases, which all are characterized by a chronic low-grade inflammation (Medzhitov 2008).

The classic symptoms of acute inflammation are *rubor* (redness), *calor* (heat), *tumor* (swelling) and *dolor* (pain). Usually, also *fuctio laesa*, the loss of function, is associated to this list. These classic symptoms of inflammation can be explained with the activation of several biological signaling systems as reviewed by several authors (Nathan 2002, Serhan and Savill 2005, Medzhitov 2008). The hallmarks of acute inflammation are increased blood flow, vascular permeability, leakage of plasma proteins and the extravasation of neutrophils to the inflamed tissue. A fast response to inflammation is based on the cells already in the tissue, such as mast-cells and macrophages. Upon inflammation, mast-cells produce many inflammatory mediators, such as histamine, eicosanoids and tryptases. These mediators are responsible for the vasodilatation and the accumulation of fluids in the tissue. The vasodilatation causes classic symptoms, for example heat and redness. The swelling of the inflamed tissue is caused by the accumulation of the leaking plasma from disrupted vessels, which in turn causes pain when the tissue stretches. In general, the pain and swelling leads to the loss of function of the inflamed organ. Tissue resident mast-cells produce also a tumor necrosis factor (TNF), which causes neutrophils to accumulate. Neutrophil recruitment to the inflamed tissue is fast and is enabled by an upregulation of the expression of the adhesion molecules. The recruitment of neutrophils begins when they move closer to the vascular wall. After this, they adhere to the endothelium by the multistep adhesion cascade, which is reviewed in chapter 2.3. Once neutrophils have adhered they transmigrate into the inflammatory site where they phagocyte microbes and/or destroy resident cells. Other cells found in the inflammatory site are the mononuclear cells, the macrophages and lymphocytes. Also the complement system starts to function and the adaptive immune response of the body is activated. Many inflammatory cells start to produce mediators, including various cytokines, chemokines and metabolisms, products of arachidonic acid, as well as vasoactive amines, which further increase the inflammatory stimuli.

The inflammatory response proceeds fast and increases over time (Nathan 2002, Serhan and Savill 2005). Usually acute inflammatory reactions can be beneficial, because they lead to the inhibition of bacterial growth, dilution of the toxins, accumulation of the antibodies and transportation of the nutrients and oxygen to the inflamed tissue. On the other hand, the inflammatory stimuli can be harmful, causing the degradation of normal tissue and swelling. After the acute inflammation has ceased, tissue can regenerate or the inflammation endures as chronic. The acute inflammation can also lead to the formation of an abscess or fibrosis. The inflammatory response is considered as chronic when it has lasted for several weeks or months (Stephenson TJ. 2004). Vasodilatation and vascular permeability are not that noticeable anymore. The reasons for chronic inflammation are, for example, foreign subjects in the body, and autoimmune reactions, such as rheumatoid arthritis (RA). Also prolonged bacterial inflammations, such as *Mycobacterium tuberculosis*, can lead to chronic inflammation.

2.2 LINK BETWEEN INFLAMMATION AND CANCER

There is an increasing amount of evidence linking inflammation and cancer. This phenomena is reviewed by several authors (Balkwill and Mantovani, 2001, Coussens and Werb 2002, Balkwill and Coussens 2004, Mantovani 2005, Mantovani et al. 2008). The inflammatory component in tumor tissue is not a novel finding. Already in 1863, Virchow suggested that chronic inflammations are the basis of many cancers. Epidemiological studies have shown that some inflammatory diseases increase the risk of developing malignant growths (including bladder, cervical, gastric, intestinal, esophageal, ovarian, prostate and thyroid cancer). An inflammatory state, which is caused by bacterial or viral infections, may precede many of these cancers (Balkwill and Mantovani 2001, Coussens and Werb 2002). A Hepatitis C infection is associated with liver carcinoma and a *Helicobacter pylori* infection is associated with gastric cancer. Some viruses, such as the human papillomavirus, hepatitis B-virus and Epstein-Barr virus can add their own oncogenes to the genome of the infected person. Nevertheless, only small portions of the infected people develop cancer. Also prolonged chronic autoimmune disease can give rise to a malignant growth. By treating the inflammatory component of the cancer, the detection rate of cancer can be diminished and the cancerous growth controlled. For instance, non-steroidal anti-inflammatory drugs have been shown to reduce the risk of certain cancers and reduce mortality (Mantovani et al. 2008).

The inflammatory component contributes to cancer development, either by the intrinsic or extrinsic pathway (Mantovani et al. 2008). In the intrinsic pathway, genetic events, such as the activation of the oncogenic mutations, chromosomal rearrangement or amplification, and the inactivation of the tumor suppressor genes, take place. Genetically transformed cells produce inflammatory mediators, even though there is no primary inflammatory disease. In the extrinsic pathway, inflammatory or infectious conditions increase the risk of developing cancer in certain organs. These two pathways result in

the activation of the transcription factors, mainly the nuclear factor kappa-light-chain-enhancer of activated B cells (NF-κB), signal transducer and activator of transcription 3 (STAT-3) and hypoxia-inducible factor 1-alpha (HIF-1α), which coordinate the production of the inflammatory mediators, including cytokines and chemokines. This creates a self-growing cycle, where these mediators recruit more leukocytes to the tissue and more inflammatory mediators are being produced by these leukocytes. This chain of events has many tumor promoting effects; cell proliferation, cell survival, epithelial-mesenchymal transition, angiogenesis and lymhangiogenesis, inhibition of the adaptive immunity and altered response to the hormones and chemotherapeutic agents. Mouse models have indicated that the elimination of the transcription factor (NF-κB) and the inflammatory mediator, TNF-α, increases the progression of cancer (Coussens and Werb 2002, Balkwill and Coussens 2004).

Mantovani and co-authors list in their review the hallmarks of cancer-related inflammation, which include the presence of the inflammatory cells and inflammatory mediators in tumor transformation, tissue remodeling, angiogenesis and tissue repair (Mantovani et al. 2008). In addition to the tumor cells, there are many different inflammatory cells in the tumor stroma. An excess of these inflammatory cells and inflammatory cytokines and chemokines promotes the development of the tumors (Coussens and Werb 2002, Balkwill and Coussens 2004, Mantovani et al. 2008). A leukocyte infiltrate is present in most, if not in all tumor tissue. Tumor infiltrating leukocytes may consist of neutrophils, dendritic cells, macrophages, eosinophils and mast cells. Tumor associated macrophages (TAMs) are the largest and most important inflammatory component in the tumor tissue. TAMs have a dual role in cancer tissue (Balkwill and Mantovani 2001, Coussens and Werb 2002, Mantovani et al. 2008). TAMs have been described as obligatory partners in tumor cell migration, invasion and metastasis. The M2 cell type of TAMs and other inflammatory cells in tumor tissue have tumor promoting effects. They may be angiogenic, lymphangiogenic and promote metastasis. The inflammation in the tumor microenvironment has many tumor promoting effects, but the inflammatory cells are also tumor suppressive, for example, they help the body to fight against the cancer. This is where the M1 type of macrophages comes into the picture. Appropriately activated macrophages can kill the tumor cells. NF-κB has been shown to play an important role in the management of balance between tumor promoting M2 type and tumor suppressing M1 types of macrophages (Balkwill and Coussens 2004). However, the exact mechanism of how the balance is shifted is not completely known.

Chemokines have been shown to contribute to the behavior of the inflammatory component in tumor tissue, especially in the invasion and metastasis (Balkwill and Mantovani 2001, Coussens and Werb 2002, Mantovani et al. 2008). Chemokines are small soluble molecules that guide cell traffic. Chemokines attract leukocytes to the tumor tissue, which further enhances chemokine and cytokine production. Many cancer cells express chemokine receptors and use chemokines to help their migration and survival during metastasis. Tumor cells can also exploit the adhesion molecules during

metastasis (Coussens and Werb 2002). Selectins are the class of adhesion molecules that iniate the multistep adhesion cascade of leukocytes by recognizing their counter receptor sialyl-Lewis X carbohydrate structure. Many epithelial tumor cells producing large quantities of sialic Lexis-X carbohydrate are highly metastatic.

2.3 THE MULTISTEP ADHESION CASCADE FOR EXTRAVASATION OF LEUKOCYTES TO THE INFLAMED TISSUE

One of the key events in inflammation is the extravasation of the inflammatory cells to the tissue. This is a tightly controlled multistep process, which exploits specific receptor pairs in the surface of the inflammatory cells and in the inflamed endothelium. Several adhesion molecules responsible for this event have been identified. Originally, the leukocyte adhesion cascade to the endothelium was described as a three step model (Butcher 1992, Springer 1994, Butcher and Picker 1996). In short, this cascade can be divided into the following steps. First, the selectin mediated rolling is followed by the chemokine mediated activation and the final step is the integrin-mediated arrest. Recently, additional steps have been suggested for this cascade. The multistep adhesion cascade for leukocyte extravasation is represented in Figure 1. The steps have been further defined to tethering, rolling, activation, adhesion, crawling and transmigration (Luster et al. 2005, Sackstein 2005, Ley et al. 2007). Also, more focus has been paid to the regulation of adhesion molecules and to what happens to the cells after arrest, when they start the intravascular crawling and transmigration takes place.

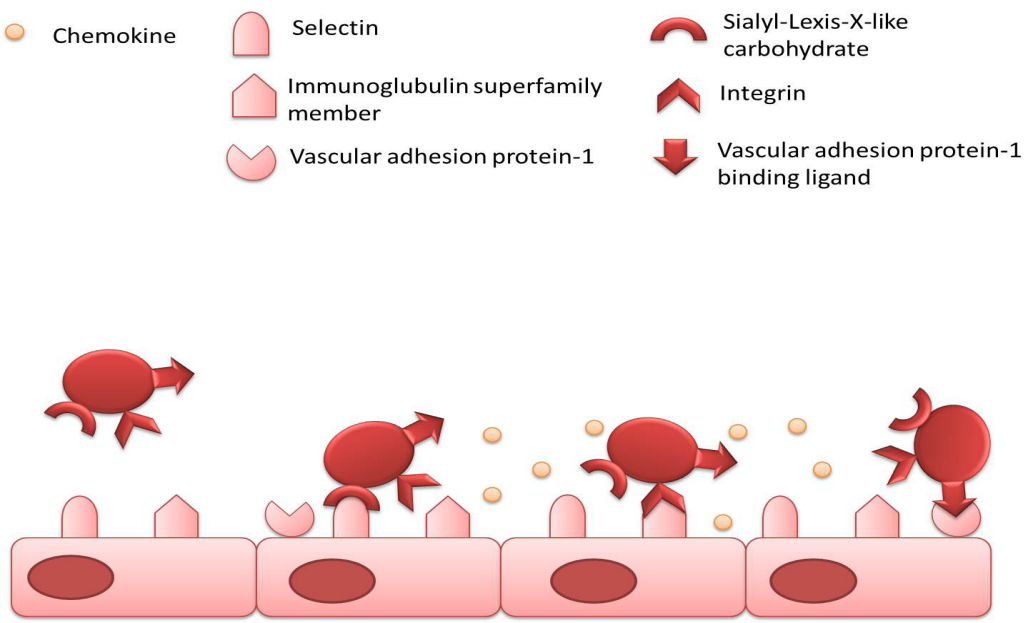

Figure 1. The multistep adhesion cascade controls the recruitment of the leukocytes to the tissue.

The blood flows in circulation at a high speed. Despite the fast velocity of the cells passing the endothelium, the inflammatory cells are able to find their target and bind to the endothelium. This event begins with the rolling phase, where inflammatory cells bounce along the endothelium and are slowed down (Ley and Kansas 2004, Luster et al. 2005, Ley et al. 2007). Rolling is mediated by L-, P and E-selectins. L-selectin is found on most circulating leukocytes and is the most important molecule at the beginning of the adhesion cascade. E- and P-selectins are endothelial adhesion molecules and they are induced during inflammation. The selectins bind to the sialyl-Lexis-X-like carbohydrate structure, the best studied and most significant being the P-selectin glycoprotein ligand-1 (PSGL1). PSGL1 is expressed in almost all leukocytes and it does not function unless glycosylated properly. Although PSGL1 was originally described as a P-selectin ligand, it is a ligand for all selectins. Selectins form transient bonds that last only a few seconds or less to slow down the leukocyte. L- and P-selectin require shear stress, the force formed by blood flowing in the vessels, to maintain the function.

Leukocyte arrest during rolling is iniated by chemokines and mediated by the binding of leukocyte integrins to immunoglobulin superfamily members, such as ICAM-1 and VCAM-1 in the endothelium (Ley and Kansas 2004, Luster et al. 2005, Ley et al. 2007). Integrins are a family of two dozen hetorodimers, containing an α- and a β-unit. Integrins that are the most relevant to arrest belong to β_1-integrin (the most studied member is the very late antigen 4; VLA4) and β_2-integrin (lymphocyte function-associated antigen; LFA1) subfamilies. All circulating leukocytes maintain their integrins in mostly inactivated states. Before the integrins can form firm bonds to their endothelial targets, they need to be activated by G-protein coupled receptors, which are likely transmembrane receptors of the chemokine family. Chemokine induced signaling changes the conformation of the integrins from a bent low affinity form to an extended active form. The chemokine system activates the leukocyte adhesion to the endothelial cells and provides directions for the leukocyte migration.

Once the leukocyte has attached, it will crawl on the endothelial cell surface to find a proper place for transmigration to the tissue (Ley and Kansas 2004, Luster et al. 2005, Ley et al. 2007). This must happen with as little interruption as possible. There are three barriers leukocytes must pass through before entering the tissue: the endothelial cell, the endothelial-cell basement membrane and the pericytes. Two routes of migration through the endothelium have been described, a paracellular and a transendothelial route. The paracellular route, where the leukocytes use the junctions between endothelial cells, is a more common one. The transcellular route is known to be used only by a few of the inflammatory cells (neutrophils and a subset of activated effector T-cells), and it takes place in the thin parts of the endothelium. In this route, the leukocytes go through the endothelial cells using special vesiculo-vacuolar organelles, which form passages inside the endothelial cell and are thought to function as a door for the leukocytes through the endothelial cell. The migration in the tissue can take place through the gaps between the pericytes and through areas of least density in the cellular matrix. The basement membrane and the extracellular matrix of stromal cells form the last barrier for the migrating leukocytes. Many of the inflammatory cells may use their proteases, as well

as the cellular matrix, destroying enzymes in order to pass through these final barriers on their way to the target tissue.

2.4 VASCULAR ADHESION PROTEIN-1 (VAP-1)

2.4.1 STRUCTURE AND LOCALIZATION

In 1992, Salmi and Jalkanen identified a novel adhesion molecule (Salmi and Jalkanen 1992). This discovery was made by producing monoclonal antibodies (mAbs) against human synovial vessels. One antibody, 1B2, stained veins in the synovia, as well as in the high endothelial venules (HEV) in peripheral lymph nodes and in the tonsils. This antibody also decreased the binding of the lymphocytes to veins in inflamed synovia. The target of this antibody was shown to be none of the known adhesion molecules, thus leading to the discovery of a novel adhesion molecule, which was named vascular adhesion protein-1 (VAP-1).

VAP-1 is a membrane bound homodimer with the molecular weight of app. 90 kDa/each monomer (Salmi and Jalkanen 1996). Figure 2 shows the schematic structure of VAP-1. The crystal structure of VAP-1 has been solved (Airanne et al. 2005). The molecule is a heart-shaped fold that contains a transmembrane domain (D1) and extracellular domains (D2-D4). The D4 domain includes an active site buried deep in the globular head of the molecule. Entry into the active site is blocked by leucine number 469, which functions as the guardian amino acid. The D4 domain has many conserved amino acid residues, and these amino acids are all involved in the catalytic reaction or the generation of the active site. The heart of the active site is the topaquinone (TPQ) that is the co-factor necessary for enzymatic activity. The active site is large enough to accommodate an amino acid side chain and might interact with a larger molecule, such as a peptide or protein ligand. VAP-1 contains several sites for glycosylation. The glycosylation is needed for VAP-1 to function properly during leukocyte adhesion.

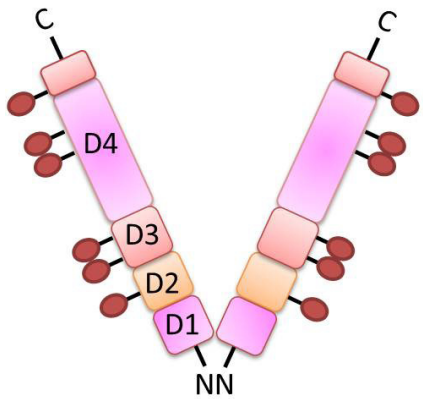

Figure 2. Schematic structure of VAP-1.

VAP-1 is also found in other tissues in addition to the inflamed synovia (Salmi et al. 1993). Under normal conditions, it can be found in several lymphoid tissues, such as HEVs in tonsils and peripheral lymph nodes. In non-lymphoid organs, VAP-1 is detected in the endothelial cells of a few small sized venules and in the smooth muscle layer of larger vessels (aorta and vena cava). In the kidney, intratubular vessels express VAP-1. In the central nervous system and in the periphery, some occasional venules are VAP-1 positive. Skeletal muscle cells are VAP-1 negative. In the heart, VAP-1 is expressed in the endothelial cells of the endocardium and in some vessels in the myocardium. The liver is also VAP-1 positive and VAP-1 has been shown to be expressed throughout the hepatic vascular and sinusoidal endothelium, and expression seems to not be up-regulated during liver inflammation in man (McNab et al. 1996). VAP-1 is an important mediator of lymphocyte and CD16+ monocyte migration to the liver and this activity can be blocked with the small inhibitors of enzymatic activity (Lalor et al. 2002, Aspinall et al. 2010). VAP-1 is absent from the surface of leukocytes, fibroblasts and epithelial cells (Salmi et al. 1993).

2.4.2 DUAL FUNCTION MOLECULE

VAP-1 participates in the recruitment of the leukocytes to the endothelium, functioning as an adhesion molecule. It plays a role during the rolling, adhesion and transmigration steps (Salmi and Jalkanen 2001). The current working hypothesis for leukocyte binding to VAP-1 is a dual mode of function, as described by Salmi and Jalkanen (Salmi and Jalkanen, 2011). The leukocyte first makes contact with VAP-1 expressed on the endothelial cells by using its counter receptor to interact with the surface of VAP-1; this part is played by the VAP-1 epitope(s) recognized by certain mAbs. After this initial contact, an amine in the surface of the leukocyte binds into the substrate channel of VAP-1. This leads to an enzymatic reaction between the leukocyte substrate with the endothelial VAP-1. The enzymatic reaction leads to the formation of an aldehyde and the release of biologically active hydrogen peroxide and ammonium. Thus, VAP-1 has an enzymatic function in addition to its adhesive function. These events are related and also the enzymatic function is needed for lymphocyte binding (Stolen et al. 2004). The blocking of the antibody binding site with anti-VAP-1 mAbs, as well as the inhibition of the Semicarbazide sensitive amine oxidase (SSAO) activity, reduce the number of adherent cells under a flow condition (Salmi et al. 2001).

The cloning and sequencing a gene encoding VAP-1 revealed several common features with SSAO (Smith et al. 1998). SSAOs (EC 1.4.3.6.) are a class of copper-containing amine oxidases, which use as substrates, for example, benzylamine, methylamine, and they are inhibited with semicarbazide and hydroxylamine (Lyles 1996, Jalkanen and Salmi 2001, Boomsma et al. 2005). In man, methylamine and aminoacetone have been reported to be natural substrates, and SSAOs have many functions, such as amine catabolism and glucose uptake. The active site in the SSAO enzyme is TPQ, which is a posttranslational product of tyrosine. The SSAO reaction is divided into two separate

half reactions; one reductive and other oxidative. In the first reaction, the amine group reacts with the co-enzyme TPQ in the active site and produces a Schiff base between the substrate and TPQ. During the first half reaction, the substrate is modified to an aldehyde. In the second half reaction, the reduced TPQ is reoxidized by Cu^{2+} and O_2 and H_2O_2 and NH_3 are released.

The main site of SSAO enzyme activity is found in blood vessels, such as the aorta, but also in adipose tissue and in smooth muscle cells (Lyles 1996). SSAO can be found in large amounts in the plasma membrane of the adipocytes and SSAO gene expression is induced during adipogenesis (Zorzano et al. 2003). Vasculature is suggested to be the main source of circulating plasma SSAOs. In healthy adults, plasma SSAO activity is quite stable, although the activity varies with age, being the highest before the age of 16 years. Previously, it has been shown that SSAOs may protect against the negative effects of amines (Boomsma et al. 2003, Boomsma et al. 2005). SSAO activity has also been associated with apoptosis and atherosclerosis. Diabetes mellitus is associated with elevated plasma SSOA activity, even more in the severe forms of the disease when patients start to show complications, such as neuropathy, retinopathy and nephropathy (Gökturk et al. 2003). Also cognitive heart disease is associated with higher levels of SSAO in the plasma. In inflammatory diseases elevation is not constant. The amount of soluble VAP-1 increases in certain liver diseases, but remains normal in many other serious inflammatory diseases, such as rheumatoid arthritis (RA) or inflammatory bowel disease (IBD) (Kurkijärvi et al. 2000). SSAO levels are decreased in some forms of cancer, such as lung cancer. Also, in the metastatic forms of skeletal cancer patients have elevated plasma SSAO levels in comparison to those without metastasis. (Boomsma et al. 2003)

The origin of SSAOs remained unclear until the source of this enzyme activity was linked to the soluble form of VAP-1 (Stolen et al. 2005). Soluble VAP-1 is shed from the cell surface, probably by proteases (Abella et al. 2004). Sources of soluble VAP-1 have been confirmed to be at least endothelial and adipose tissue (Stolen et al. 2004, Stolen et al. 2005). The observations about the levels of soluble VAP-1 have been very similar to the documented findings about SSAO activity. The biological function of SSAOs remained unknown until it was discovered that VAP-1 is the source of this enzymatic activity.

2.4.3 VASCULAR ADHESION PROTEIN-1 IN SIGNALLING

The adhesive function of VAP-1 is regulated in at least three different ways (Salmi et al. 2001). Firstly, the amount of biologically active VAP-1 in the endothelium is regulated. VAP-1 is stored in intracellular granules under normal conditions and translocated to the lumen of the cell with a maximal surface expression at 8 hr as a response to an inflammatory stimulus. Secondly, VAP-1 is not alone sufficient for lymphocyte binding. Thus, the adhesive function of VAP-1 is dependent on other adhesion molecules.

Thirdly, the VAP-1 counter receptor/substrate is found only in certain subpopulations of leukocytes.

VAP-1 also plays a role in the regulation of other adhesion molecules. Lymphocyte adhesion was shown to increase upon the activation of VAP-1 on liver endothelium in a NF-κB dependent way (Lalor et al. 2007). NF-κB activation was shown to lead to an increase of transcription of adhesion-related genes such as E-selectin and CXCL8 (IL-8) and their expression at the protein level. The expression of mucosal addressin cell adhesion molecule-1 (MadCAM-1) was also increased *in vivo* in a VAP-1/SSAO dependent way (Liaskou et al, 2011). In addition to the adhesion molecule modifying function, VAP-1 has been shown to induce apoptosis by activating the mitochondrial apoptotic pathway and tumor suppressor p53 (Sole et al. 2008).

2.4.4 VASCULAR ADHESION PROTEIN-1 IN THE INFLAMMATION

As stated earlier, VAP-1 is practically absent in normal endothelium and is induced upon inflammation (Salmi et al. 2001). The early translocation of VAP-1 onto the endothelial cell surface within an hour after the stimulus suggests that the function of VAP-1 may be connected to the early recruitment of polymorphonuclear leukocytes. Even though VAP-1 seems to play an important role in the early events of inflammation, the expression of VAP-1 on the cell surfaces stays constant for a longer time period, suggesting that VAP-1 can still be targeted after the first phase of inflammation, and making it a promising target for anti-adhesive therapy (Jaakkola et al. 2000).

Several animal models have been used to obtain knowledge of the role of VAP-1 in human pathologies. VAP-1 has been shown to mediate lymphocyte binding to the vascular endothelium in rejected kidney allografts, as well as in the liver allograft in rats (Kurkijärvi et al. 2001, Martelius et al. 2004). VAP-1 is expressed in the mouse pancreas during the development of diabetes and anti-mVAP-1 antibody treatment prevents the development of diabetes (Merinen et al. 2005). VAP-1 has also been shown to play a role in neurological diseases such as forebrain ischemia and in experimental autoimmune encephalitis (EAE), which is a rodent model for human multiple sclerosis (MS) (Xu et al. 2006, O´Rourke et al. 2007).

VAP-1 knockout and transgenic mice are very useful for studying VAP-1/SSAO (Stolen et al. 2004, Stolen et al. 2005). Although VAP-1 deficient mice do not suffer from any spontaneous infections, they have mild but significant changes in the mucosal immune system (Koskinen et al. 2007). The neutralization of VAP-1 by drugs (mAbs or SSAO inhibitors), does not affect the ability of the host to defend itself against infections. When the drug therapy is applied, there is always some SSAO activity left (5-10 %), in comparison to VAP-1 deficient mice, where all the VAP-1/SSAO activity is absent. Thus, inhibiting VAP-1/SSAO in the treatment of inflammatory disease should not cause any problems with infections.

2.4.5 VASCULAR ADHESION PROTEIN-1 IN CANCER

Few cancers have been reported to be VAP-1 positive. The first case reported was the human hepatocellular carcinomas that are more heavily infiltrated by inflammatory cells than the colorectal hepatic metastasis in the liver (Yoong et al. 1998). VAP-1 and ICAM-1 was shown to mediate the recruitment of the tumor infiltrating lymphocytes in the liver. VAP-1 also mediated the binding of immunotherapeutic cells to the vessels of a squamous cell carcinoma of the head and neck (Irjala et al. 2001). The staining of VAP-1 in melanoma samples showed a difference between the center of the tumor and its margins, with the intratumoral VAP-1 expression being lower than that in the marginal vessels, which are characterized with the most active angiogenesis (Forster-Horvath et al. 2004).

Recently, it was shown that melanoma and lymphoma tumor growth is regulated by VAP-1 and the oxidative activity of VAP-1 is necessary for the tumor-promoting effects (Marttila-Ichihara et al. 2009). VAP-1 increases angiogenesis and promotes tumor growth by enhancing the recruitment of myeloid derived suppressor cells into the tumor. Myeloid cells are known to have several tumor promoting effects, for example, the secretion of matrix metalloproteinase 9, which can induce vessel formation. In further studies, it was noticed that VAP-1 is expressed in tumor vasculature, but not in melanoma cells (Marttila-Ichihara et al. 2010). Anti-VAP-1 antibodies decreased the amount of leukocytes in the tumors, but did not prevent the tumor angiogenesis or the tumor growth. In contrast, the inhibition of the oxidative activity of VAP-1 slowed down the tumor growth and neoangiogenesis and regulated the leukocyte (myeloid cells) recruitment into the tumors.

2.4.6 INHIBITORS OF VASCULAR ADHESION PROTEIN-1

Several inhibitors and substrates of VAP-1/SSAO have been reviewed by Dunkel (Dunkel et al. 2008). The classical approach of using small molecular inhibitors has resulted in the discovery of several inhibitors, including compounds with hydrazino functionality, such as phenylallylhydrazines (LJP-1207), hydrazino alcohols and hydrazino-indanes (BTT-2052). Compounds with other functionalities have also been suggested, for instance thiocarbamoyl derivates, carboxamides and sulphonamides, compounds with a guanidino functionality and amine and amide-based inhibitors. Novel ways to inhibit VAP-1 have also been developed. Biomolecules with a free NH_2-group to interact with the enzymatic part of VAP-1 could be used, such as aminohexoses and aminoglucosides, peptides with a lysine side-chain, aminohexoses and aminoglycoside antibiotics. Function-blocking antibodies and small interfering RNAs are also one possibility to inhibit VAP-1 function.

Several small molecular inhibitors have been developed against VAP-1. A few of these inhibitors are represented in Figure 3. Blocking the enzymatic catalytic site with the small molecular inhibitor LJP-1207 (N-(2-phenyl-allyl)-hydrazine hydrochloride) had

an effect on the adhesive function and the inhibition was dose dependent in several animal models of inflammation (colitis, paw edema, endotoxemia) (Salter-Cid et al. 2005). This SSAO inhibitor also limited the neutrophil adhesion and complete inhibition was observed in the estrogen treated ovariectomized diabetic rats during the forebrain ischemia (Xu et al. 2006). Inhibition of SSAO activity by LJP-1207 was effective in reducing EAE when dosing was delayed to the peak of the acute disease, a point when inflammatory cells have already entered the central nervous system (O´Rourke et al. 2007). The inhibitor next in line, LJP-1586 (Z-3-fluoro-2-(4-methoxybenzyl) allylamine hydrochloride), was a potent, selective, and orally active compound that showed a good therapeutic window in absorption, metabolism, excretion and toxicological studies in air-pouch inflammation and lipopolysaccharide (LPS) induced lung inflammation in rats (O`Rourke et al. 2008). The small molecular inhibitor BTT-2027 (structure not published) could block VAP-1/SSAO enzymatic activity, thus decreasing the transmigration of inflammatory cells in a rat air-pouch inflammation model (Koskinen et al. 2004). SZE5302/BTT-2052 ((1S,2S)-2-(1-methylhydrazino)-1-indanol) binds covalently and selectively to VAP-1/SSAO and showed an improvement of rat adjuvant induced arthritis (Marttila-Ichihara et al. 2006). This inhibitor was able to partially prevent tissue damage in acute lung injury by inhibiting the enzymatic activity of VAP-1 (Kiss et al. 2008). The blocking of the enzymatic activity of VAP-1 by small molecule inhibitors, such as SZE5302/BTT2052 and LJP-1586, has been shown to inhibit tumor angiogenesis and growth in mice (Marttila-Ichihara et al. 2010).

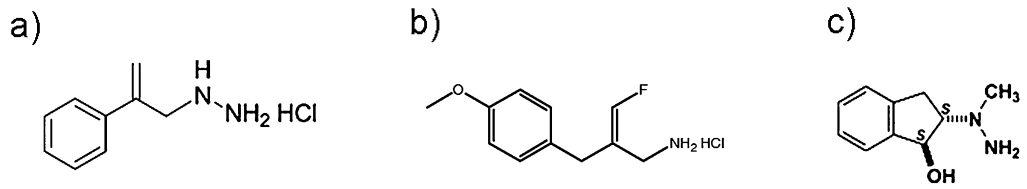

Figure 3. Structures of small molecular VAP-1/SSAO inhibitors a) LJP-1207 b) LJP-1586 and c) BTT-2052/SZE5302.

VAP-1 blocking by mAbs have shown promise in inflammation therapy. Several studies have shown the efficacy of antibody therapy in animals. The blocking of VAP-1 by mAbs was shown to lead to a dramatic reduction in the number of rolling granulocytes in the acute peritonitis model of a rabbit (Tohka et al. 2001). The migration of leukocytes to sites of inflammation could be reduced both in acute and chronic conditions in mice (Merinen et al. 2005). In mice with Con-A induced liver inflammation, Th2 cell adhesion was blocked by anti- VAP-1 mAbs (Bonder et al. 2005). A VAP-1 blockade by mAbs significantly decreased the inflammatory response in rat liver allograft rejection (Martelius et al. 2004). VAP-1 antibody therapy has also been shown to be possible in patients with nickel induced allergic contact dermatitis lesions (Vainio et al. 2005).

Using VAP-1 blocking antibody in a single dose of mouse mAb was found to be safe and well tolerated. Furthermore, there has been a development of a novel fully human antibody. In a placebo-controlled phase 1 clinical trial in rheumatoid arthritis or psoriasis patients, it was shown that the antibody did not cause any major adverse effects and suggested preliminary therapeutic potential (http://www. biotie.com/en/recearch_and_development/inflammation/vap1_antibody).

Although VAP-1 is a well-known endothelial adhesion molecule, its leukocyte counterpart has been unknown. The proposed substrate for VAP-1 has an amino sugar or free NH_2 group in an amino acid. The side chain of lysine is shown to fit into the groove of VAP-1 and interact with the catalytic site (Salmi et al. 2001). In 2009, the first leukocyte ligand for VAP-1, Siglec-10, was characterized (Kivi et al. 2009). Siglecs are a family of sialic-acid binding immunoglobulin-like lectins that are thought to promote cell-cell interactions and regulate the functions of the immune cells (Crocker 2007). Human Siglec-10 positive lymphocytes (CD19+ B-cells) were shown to use Siglec-10 as a substrate and bind to the enzymatic groove of endothelial VAP-1.

2.5 *IN VIVO* IMAGING OF INFLAMMATION USING NUCLEAR MEDICINE TECHNIQUES

Non-invasive imaging of inflammation would be a highly valuable tool (Boerman et al. 2001, Gotthardt et al. 2010). The imaging of the inflammation could aid in the diagnosis of many inflammatory conditions, such as osteomyelitis, rheumatoid arthritis, sarcoidosis, inflammatory bowel disease and fever of unknown origin. In addition to the detection of inflammatory foci, non-invasive imaging could also aid in therapy planning and monitoring. Even though there are several imaging agents used for the imaging of inflammation by nuclear medicine, none of them are specific for inflammation (Gotthard et al. 2010). These agents are summarized in Table 1.

Table 1. Imaging agents used in nuclear medicine imaging.

Imaging agent	***Accumulation mechanism***
[^{99m}Tc]- and [^{111}In]-labeled white blood cells (WBC)	Leukocyte migration
[^{67}Ga]-citrate	Binds to transferrin and extravasation to tissue due to increased vascular permeability
[^{18}F]-FDG	Increased glucose metabolism
[^{99m}Tc]-labeled biphosphonates	Binds to inflammation activated osteoblasts in the bone
[^{99m}Tc]-labeled nanocolloids	Non-specific vascular permeability and increased blood flow
[^{99m}Tc]- and [^{111}In]-labeled albumin or immunoglobulin G (IgG)	Non-specific vascular permeability and increased blood flow

Nuclear imaging modalities, single photon emission computed tomography (SPECT) and positron emission tomography (PET), offer functional and molecular information with high sensitivity. Of these two imaging modalities, PET is more sensitive and allows for quantitative imaging in a clinical setting. The comparison of these two imaging modalities has been reviewed by Rahmin and Zaidi (Rahmin and Zaidi 2008). PET allows for a better spatial resolution due to the detection of two opposite gamma quantums, whereas in SPECT the detection is based on a single photon. The greater sensitivity of PET leads to improved image quality, shorter scanning times, the option for multiple field-of-view scans and the possibility for dynamic scans. The main limitation to spatial resolution in SPECT is the instrumentation, whereas in PET it is limited, in addition to detectors, by physical factors, such as photon non-linearity and positron range. For the reconstruction of PET data into tomographical images, an attenuation correction and correction for random coincidence photons should be performed in order to provide quantitative PET data. In addition to these reconstruction algorithms, also scatter correction, correction for partial volume effect and movement correction can be taken into account to improve image quality in PET. SPECT imaging has one advantage over PET, namely dual radionuclide imaging. During a SPECT scan, two radionuclides can be measured in different energy windows. This enables the co-injection of the study agent and its control in the same study subject and allows for direct evaluation of specificity.

The accumulation of imaging agents to inflammatory foci is based on different mechanisms (Boerman et al. 2001, Gotthardt et al. 2010). For example, the uptake of Fluorine-18 (^{18}F) labeled glucose analogue (2-^{18}F-fluoro-2-deoxy-D-glucose, [^{18}F]-FDG) into inflamed tissue is caused by the increased glucose metabolism of inflammatory cells. Also tissue-specific cells, such as inflammation activated osteoblasts in the bone can be detected with Technetium-99m (^{99m}Tc) labeled biphosphonates. The characteristics of inflammation, such as increased blood flow and enhanced vascular permeability, can also be exploited in the imaging of inflammation. These unspecific events can be imaged with [^{99m}Tc]-labeled nanocolloids or [^{99m}Tc]- and Indium-111 (^{111}In) labeled proteins, such as immunoglobulin G (IgG) or albumin. In addition to these imaging agents, also Gallium-67 (^{67}Ga) labeled citrate has been used in the diagnosis of inflammatory diseases. [^{67}Ga]-citrate binds to transferrin and this complex can be extravasated to the sites of inflammation due to vascular permeability. Currently, the golden standard in nuclear medicine imaging of inflammation is autologous radiolabeled leukocytes (Boerman et al. 2001). They accumulate in the inflamed tissue by specific leukocyte migration. First, the injected radiolabeled white blood cells (WBC) adhere to the endothelium and further migrate to the tissue. The leukocytes are labeled either with ^{99m}Tc or ^{111}In, the ^{99m}Tc being the more used radionuclide due to its more optimal radiation characteristics. The accuracy of radiolabeled WBCs is excellent and is sufficient to image inflammation in a clinical setting. However, the radiolabeling of white blood cells requires a skilled technician, is laborious and involves the risk of handling contaminated blood.

The most used imaging agent in PET, the glucose analogue [^{18}F]-FDG, can also be used in inflammation imaging with high sensitivity (Love et al. 2005, Vos et al 2006). As previously mentioned, the uptake of [^{18}F]-FDG is caused by increased glucose activity in cells. [^{18}F]-FDG is transported to the cell by glucose transporters. In the cell, [^{18}F]-FDG is phosphorylated by hexokinases, but cannot be further metabolized and is trapped in the cell. The uptake of [^{18}F]-FDG is dependent on the metabolic rate of the cell and the number of glucose transporters. Since the activated inflammatory cells show an increase in the number of glucose transporters, [^{18}F]-FDG can be used in the imaging of inflammatory cells. In addition, PET as a technique allows for the quantitative measurements of [^{18}F]-FDG uptake, making it possible to evaluate the efficacy of treatment and progression of the disease. Several inflammatory/infectious conditions, such as fever of unknown origin, focal infections, osteomyelitis and vasculitis, just to name a few, have been successfully imaged with [^{18}F]-FDG (Love et al. 2005, Vos et al. 2006). Although [^{18}F]-FDG PET imaging shows potential in inflammation imaging, the uptake of [^{18}F]-FDG is not specific for inflammatory conditions and cannot be used for the differentiation of inflammation from cancer.

2.6 NUCLEAR MEDICINE IMAGING OF ENDOTHELIAL ADHESION MOLECULES

The specific imaging of inflammatory processes is a demanding task. Unspecific accumulation, as a result of an increased blood flow and enhanced vascular permeability, increases the signal in the target tissue making the specific detection difficult. As previously mentioned, none of the currently available imaging agents of inflammation are specific, thus there is a need for novel imaging agents. Targeting endothelial adhesion molecules could provide a more specific way to image inflammation and investigate endothelial activation. Table 2. shows possible targets and available imaging agents for this purpose. The imaging of adhesion molecules in inflammatory and tumor tissue may help to verify the presence of the target *in vivo*. Imaging may also speed up drug development and validation of novel drugs. If a drug compound is radiolabeled, monitoring and treatment optimization could be more efficient, since the target occupancy is possible to measure. If direct labeling of the drug is not possible, specific imaging can be used as biomarkers for measuring the changes of the drug target in the tissue of interest. In addition, both of these approaches can be used in therapy monitoring and in the evaluation of a suitable dose of new and old drugs. The combination of molecular and functional imaging is preferred in order to identify the exact location of the functional SPECT/PET signal.

Table 2. Possible endothelial adhesion molecules for nuclear imaging and available imaging agents.

Target molecule	*Imaging agent*	*Imaged condition*	*Reference*
E-selectin	[^{111}In]-or [^{99m}Tc]-labeled anti-E-selectin mAb or fragments of it	Arthritis of pig, a pig model of gout, patients with RA, patients with IBD	Keelan et al. 1994 Chapman et al. 1996 Chapman et al. 1996 Jamar et al. 2002 Bhatti et al. 1998
E-selectin	[^{99m}Tc]- labeled E-selectin binding peptide	Rat model of arthritis	Zinn et al. 1999
P-selectin	[^{99m}Tc]- labeled F(ab)2 fragment	Pulmonary embolism in beagle dog	Ji et al. 2011
VCAM-1	[^{123}I] labeled VCAM-1 antibody	Colitis in rat	Sans et al. 2001
VCAM-1	[^{123}I] and [^{99m}Tc]-labeled peptides [^{18}F]-labeled tetrameric peptide	Atherosclerosis in rabbit, atherosclerotic plaques in mice	Broisat et al. 2007 Nahrendorf et al. 2009
ICAM-1	[^{111}In]-labeled ICAM-1 antibody	Lung injury in rat	Weiner et al. 1997
Integrin $\alpha_v\beta_3$	[^{18}F]-, [^{64}Cu]- and [^{68}Ga]-labeled RGD peptides	Mouse model of chronic inflammation, acute and chronic model of inflammation in mice, atherosclerotic plaques in mice	Pichler et al. 2005 Cao et al. 2007 Laitinen et al. 2009 Haukkala et al. 2009
VAP-1	[^{123}I] labeled Anti-human-VAP-1 mAb 1B2	Animal models of skin inflammation and aseptic arthritis.	Jaakkola et al. 2000
VAP-1	[^{68}Ga]-labeled VAP-1 binding peptide	Animal model of osteomyelitis	Lankinen et al. 2008 Ujula et al. 2009

2.6.1 IMAGING OF SELECTINS

Selectins are lectins that reach over the cell membrane and participate in the rolling step of the adhesion cascade. E- and P-selectin are expressed on inflamed endothelium in several human diseases, such as RA and IBD. Preclinical studies with radiolabeled anti-E-selectin mAb confirmed the proof-of-principle of imaging for this endothelial adhesion molecule. Several animal models, such as the arthritis and gout model in pigs, proved the specific uptake of [^{111}In]-labeled anti-E-selectin mAb in the inflamed tissue (Keelan et al. 1994, Chapman et al. 1996a). In addition to gout detection in pigs, Chapman and co-workers were able to follow the kinetics of E-selectin with a labeled antibody (Chapman et al. 1996a). This [^{111}In]-labeled intact (murine) mAb was able to detect E-selectin on activated endothelium *in vivo* in patients with RA (Chapman et

al. 1996b). In comparison to human immunoglobulin G (HIG), an established imaging agent for RA, anti-E-selectin mAbs provided images in superior quality. In addition, labeled anti-E-selectin mAb showed good immunogenicity, since no human anti-mouse antibodies were detected at 12-14 days after mAb injection. Also IBD in the patient was detected with [^{111}In]-labeled E-selectin Ab and these results were comparable to radiolabeled WBCs (Bhatti et al. 1998). Even though intact mAbs showed promise in E-selectin targeting and RA imaging, they are large molecules and suffer from slow blood clearance. To address this issue, a smaller fragment of antibody was labeled with ^{99m}Tc and used in the imaging of the joint inflammation in patients (Jamar et al. 2002). [^{99m}Tc]-labeled Fab fragment of a mAb showed specific uptake as early as 4 h after the injection in comparison to a non-specific antibody. In addition to the antibody approach, a peptide labeled with ^{99m}Tc showed promise in the imaging of inflamed synovia in a rat model of arthritis (Zinn et al. 1999). Also P-selectin has been used as a target in the imaging of a pulmonary embolism in a beagle dog with [^{99m}Tc]-labeled F(ab)2 fragment of P-selectin mAb (Ji et al. 2011). However, this imaging agent is not optimal since it binds also to P-selectin in circulating platelets causing a high blood pool background.

2.6.2 IMAGING OF IMMUNOGLUBULIN SUPERFAMILY MEMBERS

Immunoglubulin superfamily is a family of cell surface receptors which participate in many tasks, including antigen recognition and binding of the complement. Five of the members in this family participate in leukocyte adhesion, interacting mainly with integrins. VCAM-1 and ICAM-1 mediate arrest in the leukocyte extravasation process and are found in the vasculature in many inflammatory conditions. To date, only preclinical studies have been published about imaging agents targeting VCAM-1 and ICAM-1. [^{111}In]-labeled antibody against ICAM-1 was specifically able to detect bleomysin induced lung injury in rats as early as 4 h after induction (Weiner et al. 1997). Several animal models, such as the experimental model of colitis in rats, atherosclerosis in the rabbit model and atherosclerotic plaques in mice have been evaluated with VCAM-1 targeting imaging agents (Sans et al. 2001, Broisat et al. 2007, Nahrendorf et al. 2009). Iodine-123 (^{123}I) labeled VCAM-1 antibody visualized specifically the inflamed colon in rats with experimental colitis in comparison to normal animals (Sans et al. 2001). [^{123}I]- and [^{99m}Tc]-radiolabeled peptides, as well as [^{18}F]-labeled tetrameric peptide targeting VCAM-1 were used in the evaluation of atherosclerosis in experimental animal models (Broisat et al. 2007, Nahrendorf et al. 2009).

2.6.3 IMAGING OF INTEGRINS

Integrins are a large member of adhesion molecules. The most extensively studied member of the integrin family is the integrin $\alpha_v\beta_3$. Integrin $\alpha_v\beta_3$ is a molecule mediating migration of endothelial cells through the basement membrane during blood vessel formation. This integrin is significantly up-regulated on activated endothelial cells during angiogenesis, but not on inactive endothelial cells. This integrin serves as a molecular marker for

tumor angiogenesis and metastasis imaging. In addition to cancer angiogenesis, integrin $\alpha_v\beta_3$ expression is also found during wound healing, RA, psoriatic plaques and during restenosis. Non-invasive monitoring of molecular processes during angiogenesis would supply helpful information for clinicians, as well as for basic scientists. The most successful imaging agents for PET and SPECT imaging of the integrin $\alpha_v\beta_3$ have been reviewed recently (Cai et al. 2005, Haubner 2006, Beer and Schweiger 2008).

Many peptides containing an arginine-glycine-aspartic acid (RGD) amino acid sequence, known to bind integrins, have been radiolabeled and studied. The first evaluation of this approach was done by Haubner and co-workers (Haubner et al. 1999). They showed that radioiodinated RGD peptides were comparable in affinity and selectivity to non-labeled structures. These peptides revealed *in vivo* receptor-specific tumor uptakes, but high hepatobiliary elimination resulted in a high radiation dose in the liver and intestine. After this initial study, RGD peptides have undergone an evolution to improve the pharmacokinetics, as well as target tissue uptake and retention, while maintaining the high affinity and selectivity and *in vitro* and *in vivo* receptor-specific binding. Several strategies have been used to improve peptide characteristics, for example, the addition of a sugar derivate to the peptide sequence, the incorporation of polyethylene glycol (PEG) spacer, the introduction of hydrophilic amino acids and multimerization (Haubner et al. 2001, Chen et al. 2004a, Chen et al. 2004b, Haubner et al. 2004, Wu et al. 2005, Zhang et al. 2005, Haubner et al. 2006, Liu et al. 2009, Dijkgraaf et al. 2011).

Galacto-RGD was the first of these peptides to be administrated in cancer patients and successfully imaged $\alpha_v\beta_3$ expression in humans with good tumor-to-background ratios (Haubner et al. 2005). In all patients, renal elimination was observed, resulting in low background activity. A great variation in tumor uptake was observed between patients and even between tumor lesions within the same patient. This suggests a great diversity of $\alpha_v\beta_3$ expression. In addition, patients with solid tumors were examined by [^{18}F]-galacto-RGD before the surgical removal of the tumor to evaluate the presence of integrin $\alpha_v\beta_3$ in the tumor tissue (Beer et al. 2006). It was shown that standardized uptake values and target-to-background ratios correlated with integrin $\alpha_v\beta_3$ staining and microvessel density. Normal tissue and tumors found to be negative in PET scans were confirmed to be $\alpha_v\beta_3$ negative. Thus, RGD-peptides can be used to image integrin $\alpha_v\beta_3$ status *in vivo*.

Although, all clinical imaging studies with RGD-peptides concern cancer patients, imaging of $\alpha_v\beta_3$ integrin may become a new biomarker for disease activity in inflammatory processes. Integrin $\alpha_v\beta_3$ expression has been confirmed in many inflammatory diseases, such as RA. In imaging studies, only preclinical studies have exploited this opportunity. The radiolabeled RGD peptide was shown to accumulate in chronic inflamed tissue in mice due to of $\alpha_v\beta_3$-specific binding, and this process can be monitored non-invasively with PET (Pichler et al. 2005). Also, the chronic phase of inflammation showed a higher uptake in comparison to acute inflammation evaluated by the ^{64}Cu-labeled tetrameric RGD peptide (Cao et al. 2007). In addition, of these chemically induced inflammatory models, radiolabeled RGD peptides have shown specific accumulation in atherosclerotic

plagues on genetically modified mice, which spontaneously develop atherosclerotic lesions (Laitinen et al. 2009, Haukkala et al. 2009).

2.6.4 IMAGING OF VASCULAR ADHESION PROTEIN-1

The first publication to show the potential of VAP-1 as a target for *in vivo* imaging was conducted by Jaakkola and co-workers (Jaakkola et al. 2000). Anti-human-VAP-1 mAb 1B2 was labeled with the chloramine T method with ^{123}I and evaluated in animal models of skin inflammation and aseptic arthritis. Inflammation was visualized and the uptake was specific in comparison to a double injected non-specific antibody.

Exploiting the knowledge of the crystal structure of VAP-1, several small peptides were modeled to fit the enzymatic groove of VAP-1. A specific lysine-containing peptide was found to be the inhibitor of SSAO activity (Yegutkin et al. 2004). The peptide, GGGGKGGGG, was tested in functional binding assays and it was shown to effectively inhibit lymphocyte-endothelial-cell interaction under conditions of flow. This peptide was labeled with ^{68}Ga and further evaluated as an imaging agent for PET imaging (Ujula et al. 2009). The preclinical testing of the VAP-1 peptide, [^{68}Ga]-DOTAVAP-P1 was promising when assessing *in vivo* stability, tissue distribution and biokinetics. *In vivo* specificity was shown in an animal model of osteomyelitis with a comparison to negative control peptides, modeled to not fit in the enzymatic loop of VAP-1, and two competitors (semicarbazide and an unlabeled peptide (DOTAVAP-P1). The study revealed a significantly lower uptake in the infected site for all negative controls. In comparison to the golden standard of PET imaging agents, [^{18}F]-FDG, [^{68}Ga]-DOTAVAP-P1 showed a slightly lower target-to-background ratio in a rat model of osteomyelitis. [^{68}Ga]-DOTAVAP-P1 was also able to accurately demonstrate the phase of inflammation in healing bones and the progress of a *S. Aureus* bacterial infection in osteomyelitic bones (Lankinen et al. 2008).

2.6.5 IMAGING OF RECEPTOR SYSTEMS WITH SMALL PEPTIDES AND ANTIBODIES

The use of biological molecules, such as peptides and antibodies, in the nuclear medicine imaging of endothelial activation is an attractive option. Endothelial adhesion molecules are ideal targets, since they are readily available in the vessel wall and can be easily accessed by an imaging agent.

Several peptides targeting receptor systems have been labeled with positron emitting radionuclides and are used in PET imaging (Gotthard et al. 2004, Mäcke et al. 2005, Reubi and Mäcke 2008, Chen and Conti 2010, Lee et al. 2010). For example, the somatostatin receptor, melanocortin receptor, gastrin releasing peptide receptor, cholecystokinin receptor, glucagon-like peptide-1 receptor, neuropeptide Y receptor and $\alpha_v\beta_3$ integrin have been imaged with radiopeptides. Small peptides fulfill many of the requirements for a good imaging agent; they are small enough for renal clearance, show fast blood

clearance and have low immunogenicity. They are rarely toxic and their stability can be improved with several chemical modifications without interfering with the target binding. Chen and Conti list several modifications, which can be used to improve the properties of peptide-based imaging agents, for example, oligomerization and multimerization (Chen and Conti 2010). Many peptides can be attached with a chelator and be labeled with radiometals. For example, ^{64}Cu and ^{68}Ga provide an easy and fast method for labeling PET imaging agents. In addition to imaging, the same peptides can also be utilized in peptide-receptor-targeted radiotherapy (PRRT) (Mäcke et al. 2005, Reubi and Mäcke 2008). The radionuclide, for example, ^{68}Ga, used for PET imaging can be replaced with a therapeutic radionuclide, such as Yttrium-90 (^{90}Y) or Lutetium-177 (^{177}Lu). The requirement for PRRT is the internalization of the peptide in the target tissue and the excretion of excess peptide via the kidneys. Thus, the main dose-limiting organ in this type of therapy is the kidney. There are several ways to lower the kidney dose. The inhibition of tubular reabsorption can be diminished by the infusion of basic amino acids, such as lysine or arginine, the modification of the peptide to reduce the positive charge of the peptide or the incorporation of a PEG spacer (Akizawa et al. 2008).

Immuno-PET exploits the specificity of an antibody and the quantitative molecular imaging with PET (Zalutsky 2006, Wu 2009, van Dongen and Vosjan 2010, Boerman and Oyen 2011). The validation of a target *in vivo* is an interesting approach, since the role of biological drugs is constantly increasing in medicine. Antibody treatments are expensive and non-effective, if the target molecule is absent in the patient. The presence or absence of a target molecule, for example, for a certain antibody treatment that can be evaluated by immuno-PET, may be used to identify patients likely to benefit from such a therapy. Molecular imaging would provide whole-body and target tissue antibody "staining" *in vivo* during the time course of disease progression without invasive sampling. Immuno-PET might provide a more accurate staging and diagnosis in comparison to direct tissue sampling; since the target molecule might be heterogeneously distributed within the tissue and a tissue sample only allows for the analysis of one location at one time point. A radiolabeled antibody can also be used in the determination of an appropriate dose for patients, since the amount of specific binding can be evaluated with PET using different doses, even in the same patient. Immuno-PET could provide us with answers to the questions, whom to treat, when to treat and with what drug to optimize personalized medicine. In addition, during the drug development process, immune-PET gives additional information about pharmacokinetics, the accumulation of an antibody in the target and other tissues, as well as about the elimination pathways of the drug. A limitation in antibody imaging is the fact that antibodies can only detect extracellular targets (Zalutsky 2006, Wu 2009, van Dongen and Vosjan 2010, Boerman and Oyen 2011). This is not a major problem, since the cell surface provides us with various targets, such as receptors, ligands, adhesion molecules, proteases and differentiation and activation targets. Intact antibodies usually have a long circulatory time, thus clearance of the background takes a long time and good quality images cannot be obtained shortly after injection of the imaging agent. This limitation has been solved

with the engineering of the intact antibody. Single-chain variable fragments, diabodies, triabodies and tetrabodies, as well as nanobodies and affibodies have been shown to improve pharmacokinetics. Usually large antibodies with long blood circulation times are labeled with radionuclides with a long physical half-life, such as ^{124}I ($t_{1/2}$ 4.18 d) and ^{89}Zr ($t_{1/2}$ 3.3 d). However, the engineered antibody fragments with faster clearance can be labeled with radionuclides having a shorter physical half-life, such as ^{64}Cu ($t_{1/2}$ 12.7 h), ^{18}F ($t_{1/2}$ 109.8 min) and ^{68}Ga ($t_{1/2}$ 67.6 min).

3 AIMS OF THE STUDY

The aim of this study was to evaluate several novel PET imaging agents targeting vascular adhesion protein-1 in different animal models of inflammation and cancer.

The specific aims of the study are the following:

I. To study whether the VAP-1 targeting peptide [^{68}Ga]-DOTAVAP-P1 was able to delineate sterile inflammation from a pancreatic adenocarsinoma xenograft. In addition, [^{68}Ga]-DOTAVAP-P1 was compared with [^{18}F]-FDG.

II. To study whether the insertion of a mini-PEG spacer would improve the PET imaging qualities of a [^{68}Ga]-DOTAVAP-P1 peptide in a sterile inflammation model.

III. To study if a novel VAP-1 ligand, siglec-9, could be used in the PET imaging of inflammation and melanoma in rodent models.

IV. To evaluate by PET the distribution, pharmacokinetics and dosimetry of a radioiodinated fully humanized anti-VAP-1 antibody in healthy rabbits.

4 MATERIALS AND METHODS

4.1 ANIMAL MODELS

All animal experiments were approved by the Lab-Animal Care & Use Committee of the State Provincial Office of Southern Finland and carried out in compliance with the Finnish laws relating to the conduct of animal experimentation. Athymic rats (rnu-rnu), Sprague-Dawley rats, wild type C57Black mice (WT), VAP-1 knockout (KO) and VAP-1 KOTG mice (mouse VAP-1 deficient mice expressing human VAP-1 as a transgene on the endothelium under a Tie-1 promoter) were used.

Rats with tumor xenografts (Study I)

Athymic nude rats (rnu-rnu) were obtained from Harlan, the Netherlands, at the age of 6 weeks. Human BxPC-3 pancreatic adenocarcinoma cells (ATCC, Rockville, MD, USA) were injected subcutaneously into the neck region of the rats and allowed to develop to the size of 1–2 cm in diameter.

Rats with sterile inflammation (Studies I, II and III)

Sprague-Dawley (Study II and III) and athymic nude rats (Study I) were subcutaneously injected with turpentine oil (Sigma-Aldrich) and inflammation was allowed to develop for 24 h prior to the PET study.

Mice with melanoma tumor (Study III)

B16 melanoma cells (Caliper Life Sciences Hopkinton, MA), were injected into the neck area of WT and KO mice for PET imaging studies and in the abdominal area for autoradiography studies. The tumors were allowed to develop for 11 days after the inoculation of the tumor cells.

Mice with inflammation (Study III)

Skin inflammation was induced with 4 drops of 5% (w/v) dinitrochlorobenzene (1-chloro-2,4-dinitrobenzene, DNCB, Sigma) in acetone applied onto the right ear of VAP-1 KO and VAP-1 KOTG mice one day before the PET imaging.

4.2 IMAGING AGENTS

4.2.1 [^{68}GA]-DOTAVAP-P1 AND [^{68}GA]-DOTAVAP-PEG-P1 (STUDY I AND II)

The DOTA-conjugated VAP-1 targeting peptides were synthesized at the Department of Chemistry, University of Turku (DOTAVAP-P1 (Study I); Ujula et al. 2009) or purchased from Almac Sciences (By Gladsmuir, Scotland, UK), ABX advanced biochemical compounds GmbH (Radeberg, Germany) and NeoMPS (Strasbourg,

France) (DOTAVAP-P1 and DOTAVAP-PEG-P1). The structures of the peptides are shown in Figure 4.

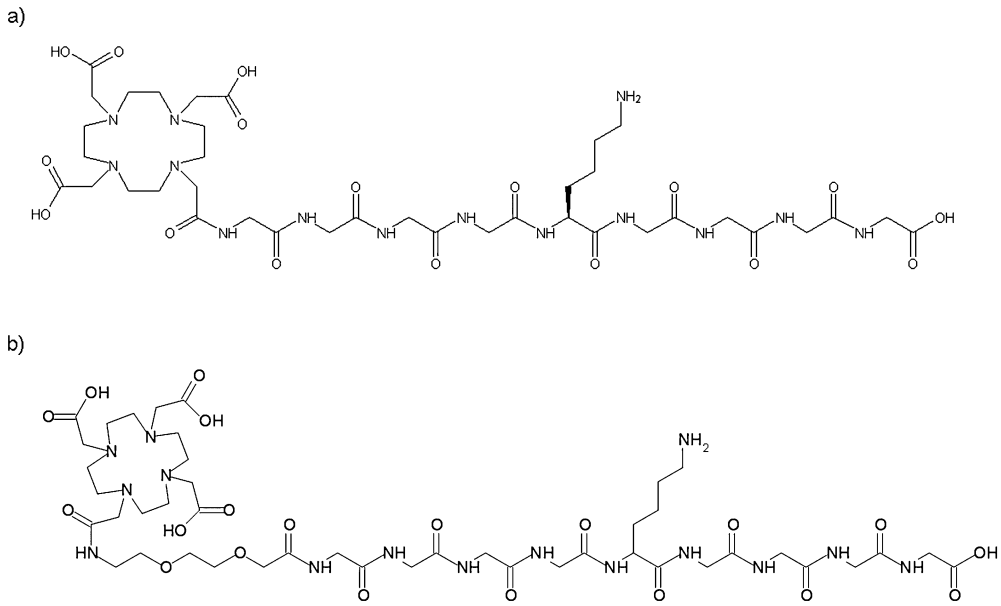

Figure 4. Structures of VAP-1 binding peptides. a) DOTAVAP-P1 with the amino acid sequence: GGGGKGGGG and a molecular weight of 989.011 g/mol, b) DOTAVAP-PEG-P1 with the amino acid sequence:GGGGKGGGG and a PEG spacer (8-amino-3,6-diooxaoctanoyl). The molecular weight of the peptide is 1133.5 g/mol.

^{68}Ga was obtained from a ^{68}Ge/^{68}Ga generator (Cyclotron Co.,Obninsk, Russia or Eckert & Ziegler, California, USA) by elution with 0.1 M HCl. [^{68}Ga]Cl_3 eluate was mixed with sodium acetate to give a pH of approximately 5.5, DOTA-peptide was added and the mixture was incubated at 100°C for 20 min. No further purification was needed. For [^{68}Ga]-DOTAVAP-P1 the radiochemical purity was determined by reversed-phase HPLC (μBondapak C18, 7.8×300 mm2, 125 Å, 10 μm; Waters, Milford, MA). The HPLC conditions were as follows: flow=4 ml/min; λ=215 nm; A=2.5 mM trifluoroacetic acid; B= 50 mM phosphoric acid. For A/B gradient: 0–8.5 min 100/0 and 8.5-16 min 0/100. [^{68}Ga]-DOTAVAP-PEG-P1 the HPLC conditions were slightly different and as follows: flow rate = 4 ml/min, λ = 215 nm, A = 2.5 mM trifluoroacetic acid, B = acetonitrile and C = 50 mM phosphoric acid. The linear A/B/C gradient was 100/0/0 for 0 to 3 min, 40/60/0 for 3 to 9 min, and 0/0/100 for 9 to 16 min. The radio-HPLC system consisted of LaChrom instruments (Hitachi; Merck, Darmstadt, Germany): pump L7100, UV detector L-7400 and interface D-7000; an on-line radioisotope detector (Radiomatic 150 TR, Packard, Meriden, CT, USA); and a computerized data acquisition system.

4.2.2 [^{68}GA]-DOTA-SIGLEC-9 PEPTIDE AND ITS CONTROL PEPTIDE (STUDY III)

DOTA-conjugated Siglec-9 peptide with a PEG spacer was purchased from Almac Group (Craigavon, United Kingdom). The control peptide was synthesized at the Department of Chemistry, University of Turku. The structure of the Siglec-9 peptide is shown in Figure 5.

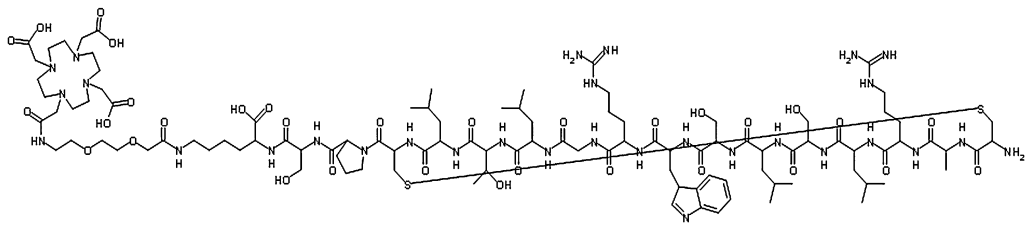

Figure 5. Structures of the VAP-1 binding DOTA-Siglec-9 peptide with the amino acid sequence: CARLSLSWRGLTLCPSK and a PEG spacer (8-amino-3,6-diooxaoctanoyl). The molecular weight of the peptide is 2420.2 g/mol.

[^{68}Ga]Cl_3 eluate was mixed with 4-(2-hydroxyethyl)-1-piperazineethanesulfonic acid (HEPES) to give a pH of approximately 3.5-4. The DOTA-peptide was added with the [^{68}Ga]Cl_3 eluate, carefully mixed, and the mixture was incubated at 100 °C for 20 min. The control peptide was [^{68}Ga]-labeled at 90 °C for 10 min. The radiochemical purity was determined by reversed-phase HPLC (μBondapak C18, 7.8 × 300 mm, 125 Å, 10 μm; Waters, Milford, MA, USA). The HPLC conditions for the ^{68}Ga-DOTA peptide were: flow rate = 4 ml/min; λ = 215 nm; A = 2.5 mM trifluoroacetic acid (TFA); B = 30 % 2,5mM TFA/ 70% acetonitrile; and C = 50 mM phosphoric acid. The linear A/B/C gradient was 100/0/0 for 0–2 min, 40/60/0 for 2–10 min, and 0/0/100 for 11–17 min. For the negative control peptide the HPLC conditions were as follows: flow=6 ml/min; λ=215 nm; A=water; B=acetonitrile; and C=50 mM phosphoric acid. For the A/B/C gradient: 0–3 min, 100/0/0; 3–4 min, from 100/0/0 to 50/ 50/0; 4–7 min, 50/50/0; 7–8 min, from 50/50/0 to 0/0/100; 8–15 min, 0/0/100. The radio-HPLC system consisted of LaChrom instruments (Hitachi; Merck Darmstadt, Germany): pump L7100, UV detector L-7400 and interface D-7000; an on-line radioisotope detector (Radiomatic 150 TR, Packard, Meriden, CT); and a computerized data acquisition system

4.2.3 [^{18}F]-FDG (STUDY I)

[^{18}F]-FDG was synthesized as described previously (Hamacher et al. 1986). The radiochemical purity exceeded 99% and specific radioactivity was >76 MBq/nmol.

4.2.4 [^{124}I]BTT-1023 (STUDY IV)

Good manufacturing practice (GMP) grade [^{124}I]BTT-1023 was produced by MAP Medical Technologies Oy, Tikkakoski, Finland. Briefly, BTT-1023 (Biotie Therapies Corp., Turku, Finland) was mixed with a phosphate buffer, Na[^{124}I] (Ritverc GmbH, St. Petersburg, Russia) and Chloramine-T (Merck, Darmstadt, Germany). The mixture was incubated at room temperature for 10 min and purified using size-exclusion chromatography. Radiochemical purity was analyzed using thin-layer chromatography (TLC). The sample was applied on a silica gel plate (Macherey Nagel, Düren, Germany) and developed with 80% methanol for 30 min. The radioactivity on the plate was detected using a gamma counter. Radionuclide purity was analyzed using a multi-channel analyzer (Canberra Eagle plus, Canberra Co., Concord, Canada).

4.2.5 *IN VITRO* STABILITY AND SOLUBILITY

The *in vitro* stability of the [^{68}Ga]-labeled peptides (Study I-II) was evaluated in human and rat plasma. Several samples were taken during the 4-h incubation period at 37°C. Proteins from plasma samples were precipitated with 10% sulfosalicylic acid followed by centrifugation and the supernatants were filtered through a 0.45 μm filter. The resulting filtrates were analyzed by radio-HPLC.

The octanol-water distribution coefficient, logD, of the [^{68}Ga]-DOTA-peptides (Study I and II) was determined using the following procedure. [^{68}Ga]-labeled peptide in phosphate-buffered saline (PBS, pH 7.4) was added to 1-octanol. After vortexing the mixture, it was centrifuged and aliquots of both layers were counted in a gamma counter. The logD was calculated as = log10 (counts in octanol/counts in PBS).

The *in vitro* stability of [^{124}I]BTT-1023 (Study IV) was tested: 1) in a mixture of physiological saline and Tween 80 at room temperature, 2) in a cell culture medium at 37°C, 3) in rabbit plasma at 37°C, and 4) in human plasma at 37°C. Samples were taken at 1, 2, 24, 48 and 72 h after incubation, and analyzed by radio-thin layer chromatography (TLC) and precipitation methods. Subsequently, the fraction of intact [^{124}I]BTT-1023 was calculated. For radio-TLC, the silica gel plate (Merck, Darmstadt, Germany) was developed with 80% methanol for 15 min. After the run, the TLC plate was briefly air-dried, and exposed to a phosphor imaging plate (Fujifilm BAS-IP MS2025; Fuji Photo Film Co, Ltd., Kanagawa, Japan), for approximately 24 hours. The identification of compounds in the samples was based on the comparison of the retardation factor (R_f) values of intact [^{124}I]BTT-1023 and free ^{124}I, applied on the same plate as the samples. The stability of [^{124}I]BTT-1023 was assessed by means of protein precipitation as well. All the proteins in the plasma sample were precipitated with acetonitrile and pelleted by centrifugation. The radioactivities of the pellet and supernatant were measured with a gamma counter (1480 Wizard 3", Wallac, Turku, Finland). [^{124}I]BTT-1023 was precipitated along with other proteins and free ^{124}I remained in the supernatant.

4.3 VAP-1 BINDING OF RADIOLABELED ANTIBODY

In Study IV, the immunoreactivity of [^{124}I]BTT-1023 was evaluated by target-ligand interaction measurements with an automated rotating radioimmunoassay (RIA) apparatus (LigandTracer Yellow, Ridgeview Instruments AB, Uppsala, Sweden). The principle of the LigandTracer is presented by Björke and Andersson (Björke and Andersson 2006). Shortly, the VAP-1 transfected cells were allowed to attach to the cell dish. [^{124}I]BTT-1023 was added to the cell medium and RIA data were collected up to 60–100 minutes. When the [^{124}I]BTT-1023 binding reached its plateau, the medium was removed, the cells were washed with a fresh medium, and the retention of [^{124}I]BTT-1023 on the cells was measured. To verify VAP-1 specific binding of [^{124}I]BTT-1023, similar experiments were performed with mock transfected cells. In addition, competition experiments with a 100-fold excess of unlabeled BTT-1023 along with [^{124}I]BTT-1023 were performed.

4.4 PET IMAGING

4.4.1 PRETREATMENT

In Study I, the animals fasted for 2–4 h prior to the injection of the tracer, because fasting is essential for ^{18}F-FDG PET studies. In other studies, no pretreatment was used.

4.4.2 ANESTHESIA

In Study I, the animals were anesthetized by an intraperitoneal injection of a mixture of midazolam (Midazolam-hameln, Hameln Pharmaceuticals, Hameln, Germany) and fluanisone plus fentanyl citrate (Hypnorm, Janssen Pharmaceutica, Beerse, Belgium). In further studies (II and III) rats and mice were anesthetized with isoflurane. In Study IV, rabbits were sedated and anesthetized with a subcutaneous injection of a mixture of medetomidine hydrochloride (Domitor, Orion Pharma, Espoo, Finland) and ketamine (Ketalar, Pfizer, Helsinki, Finland). For initial 2-h scanning, the rabbits were intubated and the anesthesia was maintained with isoflurane. For the subsequent 20-min scans, the rabbits were anesthetized with a medetomidine-ketamine mixture.

4.4.3 PET STUDIES

In Studies I-III, rats were imaged with a high-resolution research tomograph (HRRT) PET camera (Siemens Medical Solutions, Knoxville, TN, USA). This HRRT is a dedicated brain and small animal PET scanner with a resolution of 2.5 mm in the center of the field of view and 3.4 mm at the edge of the field of view (de Jong et al. 2007). Two rats were imaged at the same time. They were kept on a warm pallet during the imaging procedure. In study III, mice with tumors and mice with inflammation were imaged using Inveon Multimodality PET/CT scanner (Siemens Medical Solutions, Knoxville, TN, USA). Inveon small animal PET scanner has a resolution of 1.5 mm in the center of

the field of view and 1.8 mm at the edge of the field of view (Visser er al. 2009). In study IV, the imaging device was a whole-body PET/CT scanner GE Discovery VCT (General Electric Medical Systems, Milwaukee, WI, USA). The resolution of this camera is 4.4 mm in the center of the field of view and 5.99 mm at 10 cm off center of the field of view (Teräs et al 2007).

The details of the PET studies are presented in Table 3. The inflammation and tumor uptake was evaluated in rats bearing a pancreatic adenocarcinoma xenograft and sterile inflammation by using intravenous (i.v.) injections with [^{68}Ga]-DOTAVAP-P1 or with ^{18}F-FDG. The dynamic PET imaging started at the time of the injection (Study I).

Table 3. PET studies performed during the thesis.

Study	*Imaging agent*	*Animal model*	*Duration of scan*	*Injected radioactivity (MBq)*
I	[^{68}Ga]-DOTAVAP-P1	Turpentine induced sterile skin inflammation and pancreatic adenocarcinoma xenograft in rat	60 min	19±3
	[^{18}F]-FDG		120 min	17±7
II	[^{68}Ga]-DOTAVAP-P1	Turpentine induced sterile skin inflammation in rat	60 min	16±3
	[^{68}Ga]-DOTAVAP-PEG-P1			18±2
III	[^{68}Ga]-DOTA-Siglec-9 peptide	Turpentine induced sterile skin inflammation in rat	60 min	18±3
		Melanoma tumor in wild-type mouse and VAP-1 knock-out mouse	60 min	WT: 8±2 WT + block: 3±2 KO: 3±x2
		DNBC induced skin inflammation in hVAP-1 transgenic mouse and VAP-1 knockout mouse	30 min	KO: 7±2 KOTG: 8±3
	[^{68}Ga]-DOTA-control peptide	Turpentine induced sterile skin inflammation in rat	60 min	18±1
IV	[^{124}I]BTT-1023	Healthy rabbits	0-2, 24, 48, 72 h	52±3

In Study II effects of PEGylation were evaluated in rats with sterile inflammation i.v. injected with [^{68}Ga]-DOTAVAP-P1 or with [^{68}Ga]-DOTAVAP-PEG-P1 as a bolus via a tail vein (study II). Dynamic imaging lasting for 60 min started at the time of injection.

In Study III, the whole-body distribution kinetics and inflammation imaging were assessed in rats with sterile inflammation by using an i.v. administered [^{68}Ga]-DOTA-

Siglec-9 peptide and control peptide. The dynamic imaging lasted for 60 min and started at the time of injection. The tumor uptake kinetics and whole-body distribution of the i.v. injected [^{68}Ga]-DOTA-Siglec-9 peptide were evaluated in WT and KO mice bearing the melanoma tumor (Study III). The specificity of the [^{68}Ga]-DOTA-Siglec-9 peptide uptake was verified by PET in competitive experiments with a 500-fold molar excess of unlabeled DOTA-peptide prior to the injection of the [^{68}Ga]-DOTA-peptide into the melanoma-bearing WT mice. The inflammation uptake kinetics and whole-body distribution of the i.v. injected [^{68}Ga]-DOTA-Siglec-9 peptide were evaluated in KO and KOTG mice.

In Study IV, New Zealand White rabbits were studied for the whole-body distribution kinetics of i.v. administered [^{124}I]BTT-1023 using *in vivo* PET/CT imaging and *ex vivo* measurements of excised tissues. [^{124}I]BTT-1023 was injected i.v. and the whole-body PET/CT scanning was performed at four different time points.

In Studies II-IV, the animals were sacrificed after the PET imaging. Various organs were collected and their radioactivity was measured by using an automatic gamma counter (Wizard). The radioactivity decay was always corrected to the time of injection. In Studies I-III, the radioactivity remaining in the tail was compensated. The radioactivity concentration was expressed as a standardized uptake value (SUV), which was calculated as the radioactivity concentration (radioactivity per gram of tissue) divided by the relative injected radioactivity expressed per animal body weight. In Study IV, the radioactivity concentration was expressed also as a percentage of injected radioactivity per gram of tissue (%IA/g) and as a percentage of injected radioactivity per organ (%IA/organ). For the validation of the quantitative study, the radioactivity of tissue samples was compared with the corresponding PET values.

4.4.4 ANALYSES OF PET STUDIES

In Studies I-IV, the quantitative analysis was performed by drawing circular regions of interest (ROI) in organs of interest. In Study IV, the quantitative analysis was performed by drawing volumes of interest (VOIs) in CT images, which was then copied to PET images. The average radioactivity concentration (kBq/ml) was extracted from the dynamic PET images using the following programs: Vinci software version 2.37,Max Planck Institute for Neurological Research, Cologne, Germany (Studies I-III), Inveon Research Workplace, Siemens Medical Solutions, USA, Inc. (Study III) and iPlan RT Image version 4.1, BrainLab AG, Feldkirchen, Germany (Study IV). The uptake was reported as SUV, which was calculated as the radioactivity concentration of the ROI divided by the relative injected radioactivity expressed per animal body weight. The radioactivity decay was always corrected to the time of injection. The radioactivity remaining in the tail was compensated (Studies I-III). Time-activity curves (TACs), representing the radioactivity concentration in the organ of interest versus time after injection, were determined accordingly.

4.4.5 BLOOD, URINE AND TISSUE HOMOGENATES ANALYSES

In Studies I-IV, blood samples were collected into heparinized tubes (Microvette 100; Sarstedt, Nümbrecht, Germany). The radioactivity of the whole blood was measured with a gamma counter (Wizard). Plasma was separated by centrifugation (2,200×g for 5 min at 4°C) and plasma radioactivity was measured. The blood-plasma ratio of radioactivity was calculated and the plasma protein binding determined by [^{68}Ga]-DOTA-peptides (Studies I-II). Plasma proteins were precipitated with 10% sulfosalicylic acid, and the radioactivities in the protein precipitate and supernatant were measured. The plasma supernatant was further analyzed by radio-HPLC to evaluate the *in vivo* stability of the [^{68}Ga]-labeled peptides as described above (Chapter 4.2.1. and 4.2.2.). The stability of [^{124}I]BTT-1023 *in vivo* was studied by radio-TLC and by protein precipitation methods as described above (Chapter 4.2.5.).

In vivo stability data were used to generate metabolite-corrected plasma TACs, which were further used for the calculation of the pharmacokinetic parameters. The area under the curve (AUC) of the plasma TAC from 0 to infinity was calculated using a non-compartmental analysis employing the trapezoidal rule. The clearance (CL) after a single i.v. bolus injection was calculated by dividing the injected radioactivity by the AUC. The plot of the natural logarithm of parent tracer concentration against time after bolus injection became linear in the end phase, as the imaging agent was eliminated according to the laws of first-order reaction kinetics. The elimination rate constant (k_{el}) was calculated as the negative slope of the linear part of the plot. The plasma elimination half-life ($t_{1/2}$) was calculated as $t_{1/2} = \ln(2)/k_{el}$. The volume of distribution (V_d) was calculated from $CL=V^* k_{el}$ and adjusted to weight. The metabolic half-lives of the [^{68}Ga]-DOTA-peptides were calculated according to the results of radio-HPLC, for example, the time point when 50% of the total radioactivity was still bound to the intact peptide (Studies I and II). The plasma distribution half-life of [^{124}I] BTT-1023 was calculated from a corrected plasma curve (Study IV).

In Study I, rats were injected with [^{68}Ga]-DOTAVAP-P1 (14.3±5.4 MBq) and killed 20 min afterwards. Samples of urine, muscle and tumor were obtained and processed for radio-HPLC analysis. Tissue samples were homogenized in 10% sulfosalicylic acid using a homogenizer (Ultra-Turrax, Ika-Werke, Staufen, Germany). Cell debris and proteins were pelleted by centrifugation (3,900× *g* for 5 min at +4°C) and the supernatant was filtered through 0.45 µm Minispike filters (Waters Corporation, Milford, MA, USA). Plasma and urine proteins were precipitated as described above. All filtered samples were analyzed by reversed phase radio-HPLC. Tissue samples from inflammation foci were not analyzed by radio-HPLC because of the presence of turpentine oil. The percentage of intact ^{68}Ga-DOTAVAP-P1 was calculated from chromatograms based on the peak areas of different radioactive species.

4.4.6 DIGITAL AUTORADIOGRAPHY

In Studies I, III and IV, the organ distribution of tracers were assessed in more detail by digital autoradiography. After dissection, the tissues of interest were immediately

frozen in dry ice (Studies I and III) or embedded in Tissue-Tec and frozen in dry ice chilled with isopentane (Study IV). Tissues were sectioned with cryomicrotome into 8 or 10- and 20-µm sections at −15°C, thaw-mounted onto microscope slides and the 20-µm sections were opposed to an imaging plate (Fuji Imaging Plate BAS-TR 2025, Fuji Photo Film Co., Ltd., Tokyo, Japan). After an exposure time of 2.5 h (Studies I and III) or 24 h (Study IV), the imaging plates were scanned with the Fuji Analyzer BAS-5000 (Fuji Photo Film Co., Ltd., Tokyo, Japan; internal resolution of 25 µm (Studies I and III) or 50 µm (Study IV). After autoradiography, the sections were immunohistochemically stained with the anti-VAP-1 antibody, or with hematoxylin and eosin (HE) for histology under the light microscope.

[^{68}Ga]-DOTAVAP-P1 radioactivity distribution in inflammatory foci and tumors was studied (Study I). Rats were injected with the [^{68}Ga]-DOTA-peptide (14.3±5.4 MBq) and killed 20 min later. The distribution of radioactivity in the tumor was studied. Mice were i.v injected with the [^{68}Ga]-DOTA-Siglec-9 peptide (3.0±0.4 MBq) and killed 15 min later (Study III).

In Study IV, samples of abdominal fat, aorta, brain, lymph nodes, lungs, liver, kidneys, smooth muscle (from the small intestine wall), lymph nodes and small intestine were used for autoradiography after *ex vivo* measurements 72 h after the injection of [^{124}I]BTT-1023 (51.6±2.5 MBq). Since the small intestine sections showed clear VAP-1 positive and VAP-1 negative regions in VAP-1 antibody staining, the distribution of radioactivity in these sections was studied in more detail. The autoradiographs were analyzed for photostimulated luminescence per unit area (PSL/mm^2) using TINA Version 2.10f, (Raytest Isotopenmessgerate GmbH). ROIs were drawn on VAP-1 positive and VAP-1 negative areas according to the immunohistochemical staining of adjacent sections. Background area count densities were subtracted from the image data and uptake values were normalized against the control site (muscle).

4.4.7 ESTIMATION OF HUMAN RADIATION DOSIMETRY FROM RABBIT PET DATA

In Study IV, the absorbed doses were calculated with Organ Level INternal Dose Assessment/EXponential Modeling (OLINDA/EXM) software (Radar, USA), which applies the Medical Internal Radiation Dose (MIRD) schema for radiation dose calculations in internal exposure. The model for a 70-kg adult male was used. The residence times derived from the rabbit data were integrated as the area under the time-activity curve. The residence times were converted into corresponding human values by multiplication with a factor to scale organ and body weights:

$$(WTB,rabbit/WOrgan,rabbit)\times(WOrgan,human/WTB,human)$$

where WTB,rabbit and WTB,human are the body weights of rabbit and human (70 kg), respectively; and WOrgan,rabbit and WOrgan,human are the organ weights of rabbit

and human, respectively. Urinary clearance was estimated using the whole-body VOIs of the PET data. A voiding interval of 4 h was used in the calculation of urinary bladder residence times.

4.4.8 STATISTICAL ANALYSES

All the results are expressed as mean(s)±standard deviation (SD) or standard error of the mean (SEM) and range. The correlations between PET imaging and *ex vivo* measurement values were evaluated using linear regression analysis. Inter-group comparisons were made using an unpaired t test. Statistical analyses were conducted using Origin 7.5 software (Microcal, Northampton, USA) or using SAS 9.1.3 statistical software (SAS Institute, Inc., Cary, NC, USA). A P value less than 0.05 was considered as statistically significant.

5 RESULTS

5.1 PROPERTIES OF THE IMAGING AGENTS

Prior *in vitro* or *in vivo* studies, the radiochemical purity of imaging agents were evaluated. The radiochemical purity of all imaging agents was >95% throughout the study, as analyzed by radio-HPLC. The *in vitro* properties of imaging agents are summarized in Table 4.

Table 4. The *in vitro* properties of VAP-1 targeting imaging agents.

	[^{68}Ga]-DOTA VAP-P1	***[^{68}Ga]-DOTA VAP-PEG-P1***	***[^{124}I]BTT-1023***
Radiochemical purity (%)	> 95%	> 95%	> 95%
Retention time (min)	6.6±0.1[1]	6.7±0.1[1]	R_f 0.05[1]
In vitro stability in human plasma, intact peptide (%)	88±3[2]	89±8[2]	94±0[3]
In vitro stability in animal plasma, intact peptide (%)	82±11[2]	90±6[2]	94±0[2]
Solubility (log*D)*	-3.30±0.07	-3.50±0.02	ND

[1] For [^{68}Ga]-DOTAVAP-P1, the HPLC conditions were as follows: flow=4 ml/min; λ=215 nm; A=2.5 mM trifluoroacetic acid; B= 50 mM phosphoric acid. For A/B gradient: 0–8.5 min 100/0 and 8.5-16 min 0/100. For [^{68}Ga]-DOTAVAP-PEG-P1; flow rate = 4 ml/min, λ = 215 nm, A = 2.5 mM trifluoroacetic acid, B = acetonitrile and C = 50 mM phosphoric acid. The linear A/B/C gradient was 100/0/0 for 0 to 3 min, 40/60/0 for 3 to 9 min, and 0/0/100 for 9 to 16 min. For [^{124}I] BTT-1023 radio-TLC, the silica gel plate was developed with 80% methanol for 15 min. [2] At 4 h after incubation in human/rat plasma, [3] At 72 h after incubation in human/rabbit plasma, ND= not determinated.

The *in vitro* stability is determinated before proceeding to *in vivo* imaging studies. The *in vitro* stabilities of [^{68}Ga]-DOTAVAP-P1 and [^{68}Ga]-DOTAVAP-PEG-P1 were very similar and both peptides were highly hydrophilic.

In Study IV, the GMP grade [^{124}I]BTT-1023 was obtained with a 60–75% radiochemical yield. The *in vitro* stability of [^{124}I]BTT-1023 was good. Deiodination, the release of free ^{124}I from [^{124}I]BTT-1023, was only modest during the course of three days. In Study IV, we performed cell binding studies and confirmed the biological activity of the radioiodinated antibody. An example of the VAP-1 binding profiles of [^{124}I]BTT-1023 and BTT-1023 reference material to rhVAP-1 is given in Figure 1a, in Study IV. The relative binding activities of [^{124}I]BTT-1023 batches were 101±28%. Binding activity results within the range of 50–150% are considered to be comparable to the reference material.

5.2 ANIMAL MODELS

5.2.1 TURPENTINE OIL INDUCED STERILE INFLAMMATION (STUDY I, II AND III)

Turpentine oil injection induced subcutaneously inflammation in each animal as confirmed by the histology (Figure 1, Study I). The HE staining demonstrated the infiltration of leukocytes and macrophages at the site of inflammation (Fig. 1c, Study I). The abscess center with few cells, including residual injected oil, exudates and cell debris was surrounded by an abscess wall. Also the dermis appeared to be inflamed. According to immunohistochemical staining, luminal VAP-1 was expressed in the inflammatory region, but not in the BxPC-3 tumor xenograft tissues (Fig. 1d, h, Study I).

5.2.2 PANCREATIC ADENOCARSINOMA XENOGRAFT (STUDY I)

All animals developed a solid tumor mass when subcutaneously implanted with BxPC-3 cells (Fig. 1, Study I). The tumor volume was 0.5±0.1 cm^3 in the [^{68}Ga]-DOTAVAP-P1 group and 0.9± 0.3 cm3 in the [^{18}F]-FDG group. The histological examination of the BxPC-3 tumor xenograft revealed mainly homogeneous, viable tumor tissue without any major necrotic areas (Fig. 1g, Study I). The xenograft displayed moderately to poorly differentiated adenocarcinoma with only few inflammatory cells.

5.2.3 MELANOMA MODEL OF MICE (STUDY III)

All animals developed a solid tumor mass when subcutaneously implanted with B16 melanoma cells. The tumor mass was 0.39±0.23 g in the VAP-1 positive WT mice group and 0.25±0.01 g in the VAP-1 negative KO mice. Our observations are in line with previous publications with this model where it was shown that VAP-1 plays a role in melanoma growth and neovascularisation (Marttila-Ichihara et. al 2009). The tumors were vascularized throughout the tumor mass, which was confirmed by PV-1 antibody staining showing the blood vessels (Fig 6F, Study III). VAP-1 staining was not co-localized with all vessels. Instead, VAP-1 staining showed the presence of VAP-1, especially at the margin of the tumor mass (Fig 6E Study III).

5.2.4 CHEMICALLY INDUCED EAR INFLAMMATION (STUDY III)

All animals developed some form of inflammatory response to dinitrochlorobenzene (1-chloro-2,4-dinitrobenzene, DNCB) treatment of the ear. VAP-1 positive transgenic mice and VAP-1 negative knockout mice were used. Since the level of VAP-1 varies between animals, the presence of VAP-1 in ear samples was confirmed in every case. The KOTG mice without clearly detectable VAP-1 expression (n=3) were excluded from the VAP-1 positive group.

5.3 PET IMAGING STUDIES

In Study I, both [^{68}Ga]-DOTAVAP-P1 and [^{18}F]-FDG were capable of visualizing all turpentine oil-induced inflammatory lesions from the surrounding tissues by PET (Figs. 2a and 3a, Study I). The BxPC-3 human adenocarcinoma xenografts were clearly visible by ^{18}F-FDG (Figs. 3a, Study I), but poorly visible with [^{68}Ga]-DOTAVAP-P1 (Fig. 2a, Study I). By *in vivo* PET imaging, the inflammation and tumor uptakes expressed as SUV were 1.06±0.41 and 0.42±0.10 for [^{68}Ga]-DOTAVAP-P1 (n=4) at 20 min after injection and 2.02±0.52 and 1.59±0.75 for [^{18}F]-FDG (n=3) at 90 min after injection, respectively (Table 1, Study I). Although, on average the inflammation uptake of ^{18}F-FDG was 1.9-fold higher and the tumor uptake 3.8-fold higher than that of [^{68}Ga]-DOTAVAP-P1, the difference was statistically insignificant. The status of VAP-1 was evaluated in the inflammation and tumor by immunohostochemistry. Representative digital autoradiographs of [^{68}Ga]-DOTAVAP-P1 distribution at the sites of inflammation and tumor are shown in Figures 1a and 1e of Study I. The distribution of ^{68}Ga radioactivity in inflammatory tissue was heterogeneous, concentrated on areas of inflammatory cells around the residual turpentine oil and adjacent skin. Lower radioactivity was seen in the turpentine oil injury site. The tumor sections revealed low but homogeneous distribution of ^{68}Ga radioactivity.

In Study II, both peptides were capable of visualizing inflammatory foci from the surrounding tissues by PET imaging (Fig. 1a, Study II). The inflammation uptakes expressed as SUVs were 0.33±0.07 and 0.53±0.01 for [^{68}Ga]-DOTAVAP-P1 and [^{68}Ga]-DOTAVAP-PEG-P1, respectively, at 60 min after injection. Inflammation-to-muscle ratios at 60 min after injection were 6.7±1.3 and 7.3±2.1 for [^{68}Ga]-DOTAVAP-P1 and [^{68}Ga]- DOTAVAP-PEG-P1, respectively. On the average, the inflammation uptake of [^{68}Ga]-DOTAVAP-PEG-P1 was 59% higher than that of [^{68}Ga]-DOTAVAP-P1, and the difference was statistically significant (P=0.047). According to the whole-body dynamic PET imaging, [^{68}Ga]-DOTAVAP-PEG-P1 showed slower renal excretion to the urine, but otherwise rather similar distribution kinetics as the original peptide [^{68}Ga]-DOTAVAP-P1 (Fig. 1b–e, Study II). The PET imaging results were verified by *ex vivo* measurements (Fig. 2, Study II). Linear regression analysis showed a reasonable correlation between *in vivo* PET and *ex vivo* tissue samples (R=0.58, P=0.023 for [^{68}Ga]-DOTAVAP-P1 and R=0.80, P<0.001 for [^{68}Ga]-DOTAVAP-PEG-P1).

In Study III, inflammation imaging was demonstrated with an experimental model of sterile inflammation as shown in Figure 5A, Study III. There was clear visualization of the inflammatory foci in the neck area, with a good target-to-background ratio of up to 60 min for [^{68}Ga]-DOTA-Siglec-9 peptide (5.88±2.28 by *ex vivo* and 6.66±1.56 by PET). PET imaging revealed that the uptake of [^{68}Ga]-DOTA-Siglec-9 peptide in inflammatory foci was fast. In comparison to a control peptide at the time point of highest radioactivity in the inflammation signal, the [^{68}Ga]-DOTA-Siglec-9 peptide inflammation-to-muscle ratio was higher, the ratio was 6.59±0.72 for [^{68}Ga]-DOTA-Siglec-9 and 5.59±0.05 for the control peptide. *Ex vivo* biodistribution studies with Sprague-Dawley rats with

inflammation showed that 60 min after an i.v. administration of [^{68}Ga]-DOTA-Siglec-9 peptide, the radioactivity was the highest in the urine (mean SUV 65.84) and in the kidneys (mean SUV 11.89), and lower radioactivity was seen in the liver (mean SUV 1.49) and inflammation (mean SUV 0.43).

To study the whole-body distribution and tumor kinetics of the [^{68}Ga]-DOTA-Siglec-9 peptide, PET imaging was performed with VAP-1 KOTG mice bearing a melanoma tumor (Study III). To clarify specificity of [^{68}Ga]-DOTA-Siglec-9 uptake, competition assays were performed in VAP-1 KOTG mice with a 500-fold mass excess of unlabeled [^{68}Ga]-DOTA-Siglec-9 peptide. PET imaging revealed a significantly lower uptake in the tumor with the presence of competing cold peptide (Figure 6A, Study III). *Ex vivo* measurements confirmed this result: tumor SUV with [^{68}Ga]-DOTA-siglec-9 peptide alone was 0.56±0.12 and 0.17±0.02 with the competition (P=0.0047). The excess of cold peptide displaced the radioactive peptide binding in all the organs to the same level as detected in the VAP-1 KO mice, except in the kidneys (Table 1, Study III). In the tumor bearing WT mice, the radioactivity concentrated in the periphery of the tumor (Figure 6B-C, Study III). It is consistent with the finding that VAP-1 expression is also highest in these areas (Figure 6D-E, Study III). The distribution of [^{68}Ga]-DOTA-Siglec-9 peptide within the tumor was studied with autoradiography. Radioactivity was clearly localized at the peripheral parts of the tumor mass and in the surrounding tissue. The PSL/mm^2 value for the VAP-1 positive region in the tumor was 265.79±118.30 and 55.59±28.00 for the VAP-1 negative region. The difference between the areas was significant. We further tested whether the [^{68}Ga]-DOTA-Siglec-9 peptide could be used to image skin inflammation in the VAP-1 KO mice and KOTG mice expressing human VAP-1 on the endothelium. The peptide was able to detect inflammation in the mouse as well (Supplemental Figure 2, Study III). As demonstrated in Supplemental Table 2 in Study III, the peptide detects human VAP-1 in many organs of the VAP-1 transgenic mice, leading to higher signals than in KO mice. *Ex vivo* measurements confirmed this. SUVs in inflammation foci were 0.34±0.06 for VAP-1 negative KO mice and 0.66±0.27 for VAP-1 positive KOTG mice. The difference was significant.

All of the ^{68}Ga-labeled peptides used in this study were able to delineate inflammation from background muscle in the expremental model of sterile inflammation in rats as seen in Figure 6. All peptides had high target-to-non target ratios (above 6) and showed fast uptake in the inflammatory foci, as well as preferred renal clearance and some uptake in the liver. The SUVs derived from PET images were 0.33±0.07, 0.53±0.01 and 0.45±0.06 for [^{68}Ga]-DOTAVAP-P1, [^{68}Ga]-DOTAVAP-PEG-P1 and [^{68}Ga]-DOTA-Siglec-9 peptide, respectively, at 60 min after injection.

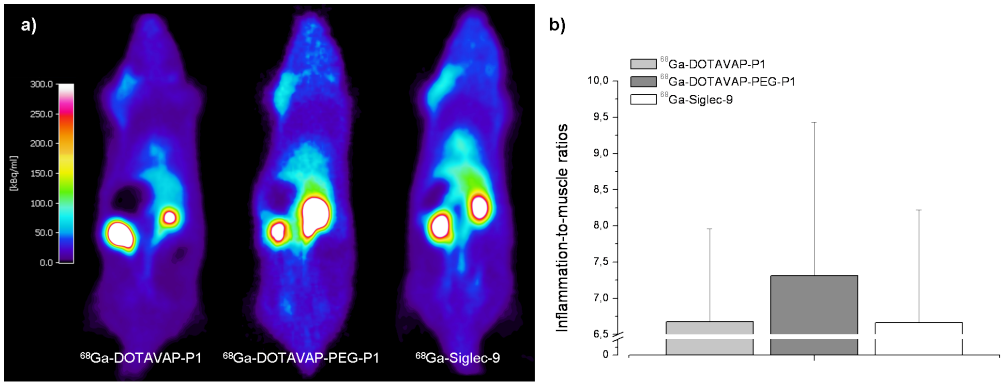

Figure 6. a) PET images of ^{68}Ga-labeled VAP-1 binding peptides. All the images are in the same radioactivity scale, scalebar shown to the left. **b)** Inflammation-to-muscle ratios obtained from PET imaging at 60 min p.i.

Instead of peptides, a radiolabeled antibody was used in Study IV to target VAP-1. Radioactivity accumulated in the liver rapidly after injection and declined slowly during the 4-day experiment. The thyroids showed a high uptake (SUV 49±14) during the day 4 scan, which is probably due to the deiodination of the antibody. Radioactivity was cleared fast from the heart. Only a small amount of radioactivity (SUV 0.6±0.2) was seen in the kidneys, which serve as the elimination route for free iodine. Table 1 and Figure 3a show the results of *ex vivo* distribution of [^{124}I]BTT-1023-derived radioactivity in rabbits at 72 h after injection. Linear regression analysis showed a good correlation between the radioactivity of tissue samples and PET values (R=0.94, Fig. 3b). The thyroid glands were excluded from the correlation due to the inaccuracy of *in vivo* PET quantification caused by the partial volume effect of small objects. The organs with the highest SUV were the thyroid glands 304.80±98.92 and the liver 8.40±3.55. Representative PET/CT images and TACs of these organs are shown in Figure 2 and Table 2.

Autoradiography analysis of ^{124}I derived radioactivity showed homogeneous distribution in the liver, lung, brain, abdominal fat, aorta and lymph node cryosections. In small intestine cryosections, the radioactivity was localized much more in the smooth muscle than in the lamina propria. These observations are in line with VAP-1 expression that is high in smooth muscle. Representative images are shown in Figure 4. According to the autoradiography of small intestine cryosections, the uptakes of [^{124}I]BTT-1023 in VAP-1 positive and VAP-1 negative areas were 4.81±2.07 and 0.93±0.61, expressed as PSL/mm^2, respectively (P<0.001).

5.4 *IN VIVO* STABILITY OF THE IMAGING AGENTS

In Study I, the *in vivo* stability of [^{68}Ga]-DOTAVAP-P1 was evaluated at 20 min after i.v. injection. According to radio-HPLC analysis, the proportion of intact [^{68}Ga]-DOTAVAP-P1 in rat plasma, muscle, tumor and urine were 56±7% (n=4), 42±3% (n=4),

61±1% (n=3) and 86±2% (n=4), respectively. This indicates that a major part of the peptide was still intact when eliminated via the urinary tract.

In Study II, the blood-plasma ratios and the plasma free fractions (f_p), for example, the fraction of total radioactivity in plasma that is unbound to plasma proteins, are summarized in Table 5. The *in vivo* stability of ^{68}Ga-DOTAVAP-PEG-P1 was significantly better than that of [^{68}Ga]-DOTAVAP-P1. The proportions of unchanged peptides in rat plasma at 60 and 120 min after injection were 19±4% and 4±1% for [^{68}Ga]-DOTAVAP-P1, and 76±18% and 49±6% for [^{68}Ga]-DOTAVAP-PEG-P1, respectively (Fig. 3, Study II). The metabolic half-lives of [^{68}Ga]-DOTAVAP-P1 and [^{68}Ga]-DOTAVAP-PEG-P1 were 24 min and 125 min, respectively. Figure 7 shows representative HPLC-grams of both peptides in rat circulation 30 and 60 min after injection.

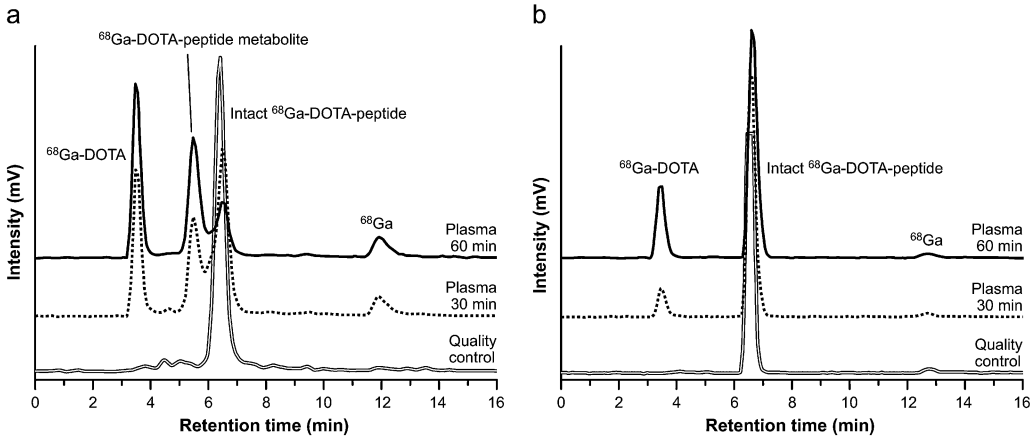

Figure 7. Representative HPLC-grams of both peptides: a) [^{68}Ga]-DOTAVAP-P1 and b) [^{68}Ga]-DOTAVAP-PEG-P1 in rat circulation 30 and 60 min after injection.

Based on *in vivo* plasma measurements, [^{68}Ga]-DOTAVAP-PEG-P1 showed significantly slower k_{el} and total CL and larger AUC values. In addition, [^{68}Ga]-DOTAVAP-PEG-P1 had a longer elimination $t_{1/2}$ than the original [^{68}Ga]-DOTAVAP-P1, although the difference was not statistically significant (Table 1, Study II).

Table 5. *In vivo* properties of VAP-1 targeting imaging agents in Sprague-Dawley rats.

	[^{68}Ga]-DOTA VAP-P1	***[^{68}Ga]-DOTAVAP-PEG-P1***
In vivo stability in rat plasma (%)[1]	19±4	76±18
plasma-free fraction f_p	0.84±0.04	0.86±0.02
Blood-plasma ratios	1.3±0.1	1.3±0.1

[1] At 60 min after injection

In Study IV, the proportion of intact [^{124}I]BTT-1023 in a rabbit at 72 h after i.v. injection was 80±10% by both precipitation and TLC methods. In the urine, at 72 h after injection, the radioactivity derived merely from the free ^{124}I. The plasma pharmacokinetic parameters were as follows: distribution $t_{1/2}$ 4.8±3.8 min, k_{EL} 0.0120±0.0021 1/h, elimination $t_{1/2}$ 58±11 h, AUC 2200±480 h*kBq/mL, CL 7.8±1.8 mL/h/kg and volume of distribution V_d 650±180 mL/kg.

5.5 ESTIMATION OF HUMAN RADIATION DOSIMETRY FROM RABBIT PET DATA

In Study IV, according to the rabbit data, the effective dose for a 70-kg man was estimated to be 3.7±1.1 mSv/MBq. Most of this radioactivity dose came from the thyroid glands, an uptake which could be blocked with an excess of iodine (i.e. potassium iodide) given prior to the administration of [^{124}I]BTT-1023. When a thyroid gland uptake of ^{124}I radioactivity is blocked, the effective dose is much lower, i.e. 0.55±0.08 mSv/MBq. This effective dose is equivalent to 21 mSv from 35 MBq and 30 mSv from 50 MBq of [^{124}I]BTT-1023 PET. The human residence times and the estimates for human dosimetry extrapolated from the rabbit data are presented in Table 3 in Study IV.

6 DISCUSSION

PET imaging of inflammation offers a non-invasive, quantitative approach to diagnosis, therapy planning and monitoring and to drug development. Nevertheless, clinical applications of this method are currently limited by the lack of specific imaging agents to visualize molecular events *in vivo*. [^{18}F]-FDG is the most used PET imaging agent in cancer and inflammation imaging. Although [^{18}F]-FDG is very useful in evaluating the increased metabolic state of tissue, it is not specific for inflammatory or cancerous processes.

The nuclear imaging of adhesion molecules provides an exciting tool for the specific detection of inflammation and cancer. Antibodies and small peptides targeting adhesion molecules have been labeled with SPECT and PET radionuclides and used in *in vivo* imaging. The most studied adhesion molecule for imaging purposes is $\alpha_v\beta_3$ integrin (Cai et al. 2005; Haubner 2006; Beer and Schweiger 2008). A specific peptide sequence, RGD, has been observed to be quite stable and have a high affinity towards $\alpha_v\beta_3$ integrin. This imaging tool has mostly been used for imaging tumor angiogenesis, since the $\alpha_v\beta_3$ is expressed in neovasculature.

In our studies, we have exploited the unique adhesion molecule VAP-1 as a target. The proof-of-concept studies regarding the usability of VAP-1 in this context have been performed by Jaakkola and co-workers (Jaakkola et al. 2000). They analyzed the *in vivo* behavior of ^{123}I-labeled chimeric mouse-human anti-VAP-1 antibody in dogs and pigs by using SPECT. These studies suggested that VAP-1 is a promising target for the *in vivo* imaging of inflammation as it is easily accessible on the endothelium upon inflammation. Previously, we have shown that the [^{68}Ga]-DOTAVAP-P1 peptide generated by molecular modeling to fit the enzymatic groove of VAP-1 is a potential imaging agent for diagnosing osteomyelitis (Lankinen et al 2008, Ujula et al 2009).

6.1 SELECTION OF IMAGING MODALITY

SPECT is more commonly used in nuclear medicine since these scanners are more frequently available than PET equipments. Although, clinical PET scanners have a higher resolution than SPECT scanners, the small animal nanoSPECT (pinhole SPECT) provides excellent resolution and is comparable to the imaging quality of small animal PET scanners. The resolution in nanoSPECT was shown to be superior over small animal PET scanner, but the sensitivity was lower than with animal PET when comparing the most used isotopes for SPECT (^{99m}Tc) and for PET (^{18}F) imaging (Cheng et al. 2010). However, clinical PET provides higher resolution images and the possibility to obtain radioactivity concentration in the tissue. Although PET is a non-invasive and quantitative imaging modality, which is able to detect small amounts of injected imaging agents in

a target organ, there are some limitations to this technology. When performing small animal imaging studies with clinical camera systems, for example HRRT, a partial-volume effect might cause a problem and possibly invalidate the *in vivo* quantitative PET data. To minimize the partial-volume effect, we used the average radioactive concentration within the ROI (kBq/ml). Although the partial-volume effect is a possible source of error, the correlation of *ex vivo* measured tissue samples and the last frames of the PET images were good. Anatomical reference would further improve image analysis.

6.2 SELECTION ON RADIONUCLIDE

The positron emitter chosen should fulfill several requirements. The decay mode and maximal energy of radionuclide should be feasible to obtain good quality PET images. The amount of β+ radiation of the radionuclide influences the image sensitivity. If the amount of β+ energy in the radiation profile is 100%, the images are more quantitative, since all of the radiation emitted by the radionuclide can be detected with the PET camera. The maximal β+ energy affects the resolution of the images, as the higher the maximal energy, the blurrier the PET image is, in theory. The half-life of the radionuclide should match the half-life of the cold compound. Ideally, the labeling protocol should be feasible, reproducible and lead to a GMP level final product. An advantage is if the labeled product can be transported to more distant locations. Several radionuclides are available for the labeling of peptides and antibodies. In these studies we have used ^{68}Ga, which matches the half-life of the peptides and ^{124}I for antibody labeling.

^{68}Ga offers a cyclotron-independent, convenient, and low-cost access to PET imaging agents. ^{68}Ga is readily available by elution from ^{68}Ge/^{68}Ga generator possessing, with a 1–2 years life span depending on uploaded Germanium-68 (^{68}Ge) radioactivity. Furthermore, ^{68}Ga has convenient characteristics, such as β+ decay 89%, Eβ+max 1.9 MeV and a sufficiently long half-life (68 min) for PET imaging. Although ^{68}Ga as a PET imaging radionuclide has several advantages, also a few limitations exist. ^{68}Ga has rather high positron energy (Eβ+max 1.9 MeV), which leads to a longer traveling time of the positron in the tissue. Thus, in theory, PET images obtained using ^{68}Ga as a radionuclide are not as optimal as the lower energy radiators, for example,^{18}F (Eβ+max 0.64 MeV). In practice, we did not observe any major differences in the comparison of the images between ^{68}Ga-DOTAVAP-P1 and [^{18}F]-FDG imaged animals (Study I).

^{124}I is produced by cyclotron with a half-life of 4.18 days. The long half-life makes it possible to ship the radionuclide to distant locations for labeling. The relatively long physical half-life also allows for the monitoring of the antibody kinetics *in vivo* for several days. The labeling chemistry of ^{124}I is rather straightforward and the physical half-life of the radionuclide is suitable for immuno-PET. To obtain proper PET images, the injected radioactivity of ^{124}I would ideally need to be higher than that of other PET radionuclides, since only 25% of the ^{124}I decay is by positron emission, with the rest being gammas and x-rays. On the other hand, the longer half-life of ^{124}I facilitates longer

acquisition of PET data, which improves the image quality. ^{124}I also has quite high positron energy in comparison to ^{18}F. This might result in poorer image quality. In our studies, the imaging quality was rather good and even small structures, such as thyroid glands, were seen as clear structured and paired separate organs (Study IV).

^{124}I has also another drawback, the intracellular dehalogenation *in vivo* by enzymes, which leads to a high uptake in thyroid glands. Thus, ^{124}I is preferred if the antibody is not internalized. The uptake of the thyroid glands can be blocked with adequate administration of cold iodine. Direct iodination is potentially damaging for the antibody due to the modification of tyrosines in Complementarity determining regions (Nikula et al. 1995). To assure that this was not the case, we tested whether the iodination process in general would destroy the binding capacity of the antibody with TRIMFA. There is a risk that the reduced binding radioiodinated antibody would not be detected with TRIMFA due to masking by the binding of unlabelled antibodies, since the entire antibody fraction is measured. Thus, we ensured that the portion of antibody that is radioiodinated is still able to bind to antigen with a Ligand Tracer. However, measurements of immunoreactive fractions using excess amounts of antigen would have been useful (Nikula et al 1999). As performed, there is a change that the LigandTracer experiment reveals only a small fraction of labelled antibody that is capable of specific binding to VAP-1 expressing cells. However, if the labeled fraction would have consisted of a large portion of damaged antibody with a diminished binding capacity to VAP-1, there would have been larger non-specific binding in LigandTracer experiments.

6.3 ANIMAL MODELS

Several animal models were used during these studies. As a preliminary screening model, sterile turpentine oil inflammation was used. This model has been validated previously by Yamada and co-workers (Yamada et al. 1995). They showed that [^{18}F]-FDG can be used for the detection of inflammatory cells and the highest [^{18}F]-FDG uptake occurs in the chronic phase of inflammation on day 4. In our study, we wanted to evaluate PET imaging agents in the acute inflammatory phase. On day 1, characteristics of acute inflammation, such as the migration of neutrophils, were seen. We confirmed the presence of VAP-1 in the inflammatory margin with immunohistochemistry.

We wanted to further evaluate the [^{68}Ga]-labeled siglec-9 peptide in other models, such as chemically induced acute dermatitis and a B16 melanoma tumor in a mouse. The DNCB induced skin inflammation has been used in pigs to study up- and down regulation of VAP-1 on the vascular wall (Jaakkola et al. 2000). This study showed that VAP-1 is translocated quickly onto the cell surface and the highest values were obtained at 8h after induction. After 24 h, the signal started to decrease. We chose the time point of 24 h after induction. At this time point, the VAP-1 signal was still strong and studies could be performed within a feasible timetable. The melanoma model in VAP-1 negative KO mice and VAP-1 positive WT mice has shown that the tumor growth is regulated

by VAP-1 (Marttila-Ichihara et al. 2009). Tumor growth was shown to be impaired in the VAP-1 deficient mice and the maximal difference between the different genotypes during the tumor development was seen 11 days after inoculation of the tumor cells. This was the time point we chose for our imaging studies.

The evaluation of [^{124}I]BTT-1023 was performed on healthy rabbits in order to calculate dosimetry and to further study the *in vivo* biodistribution of this antibody. Further studies are warranted to clarify the fate of [^{124}I]BTT-1023 in an inflammation model. Although interspecies extrapolation of biokinetic data is based on the fact that cellular structure and biochemistry are remarkably alike within animal species and BTT-1023 recognizes rabbit VAP-1, there are some limitations in using laboratory animals in dosimetry estimations. Extrapolation of biokinetic data from laboratory animals to humans is uncertain, particularly for the liver, due to the qualitative differences among species in the handling of many substances by this organ.

6.4 IMAGING STUDIES

Peptides used in these studies fulfill several of the properties required for peptides in PET imaging. These peptides show specificity to target, good target-to-nontarget ratio, rapid clearance from the blood and preferable renal excretion. They are also easy to produce. Small peptides usually have low immunogenicity and toxicity and we did not observe any acute toxicity in our studies. Also their stability can be improved with several chemical modifications without interfering with the target binding, as was done by PEGylation in Study II.

In the first study (Study I), we wanted to evaluate [^{68}Ga]-DOTAVAP-P1 in an experimental model of acute, sterile inflammation and in human pancreatic adenocarcinoma xenografts and compare the findings with [^{18}F]-FDG. Our results revealed that the uptake of [^{68}Ga]-DOTAVAP-P1 at the site of inflammation was comparable to ^{18}F-FDG. Yet, the tumor uptake of [^{68}Ga]-DOTAVAP-P1 was low in contrast to prominent [^{18}F]-FDG uptake. The results of [^{68}Ga]-DOTAVAP-P1 were in line with the expression of luminal VAP-1, which was high at the site of inflammation, but low in BxPC-3 derived tumor xenografts. Although this peptide showed specific binding *in vivo*, the half-life was relatively short (26 min) and clearance from the circulation very rapid. Also, it has remained unknown in which form the radioactivity is present in tissues. To clarify this, we analyzed also tumor and muscle homogenates by radio-HPLC. The metabolic fate of intravenously injected [^{68}Ga]-DOTAVAP-P1 in rat plasma and urine is in accordance with our previous study. The amount of intact [^{68}Ga]-DOTAVAP-P1 in the tumor was slightly higher than in plasma and muscle. We have previously published two papers regarding the [^{68}Ga]-DOTAVAP-P1 peptide (Lankinen et al. 2008, Ujula et al. 2009). The general distribution of [^{68}Ga]-DOTAVAP-P1 in the athymic rat model is in accordance with those of previously reported in Sprague-Dawley rats. In both of these rat strains, intravenously administered [^{68}Ga]-DOTAVAP-P1 exhibited rapid excretion through the kidneys to the

urinary bladder. Notable retention in the liver and very low radioactivity in the brain was observed. The high hydrophilicity of [^{68}Ga]-DOTAVAP-P1 (logD–4.5) gives an explanation for the rapid renal excretion (Ujula et al. 2009).

In the following study (Study II), we showed that the incorporation of a mini-PEG spacer in [^{68}Ga]-DOTAVAP-P1 enhanced its *in vivo* stability and improved the PET imaging of inflammation. The incorporation of a mini-PEG spacer had no apparent effect on the *in vitro* properties of the VAP-1 binding peptide; both peptides were stable in plasma incubations *in vitro* and their solubility was very similar. However, when intravenously administered, [^{68}Ga]-DOTAVAP-PEG-P1 showed significantly longer metabolic and elimination half-lives and slower total clearance compared to [^{68}Ga]-DOTAVAP-P1. Furthermore, our results revealed that while both peptides were able to visualize experimental inflammation by PET imaging, [^{68}Ga]-DOTAVAP-PEG-P1 showed a higher inflammation-to-muscle ratio than the original [^{68}Ga]-DOTAVAP-P1. The renal excretion of [^{68}Ga]-DOTAVAP-PEG-P1 was slower, resulting in significantly lower urinary bladder radioactivity in comparison to [^{68}Ga]-DOTAVAP-P1. PEGylation has been used widely for improving the *in vivo* kinetics of pharmaceuticals. However, the results of such modifications depend much on the nature of the lead compound and the choice of the PEG spacer (Wen et al. 2001, Ke et al.2004, Chen et al. 2004b, Wu et al. 2007, DeNardo et al. 2009, Liu et al. 2009a, Liu et al. 2009b). In most cases, PEGylation of radiopeptides has advantageous effects, such as increased metabolic half-life, decreased kidney uptake, and improved targeting for high-quality imaging. However, disadvantageous results have also been reported, for example, the insertion of a long PEG chain may induce a higher liver uptake and reduce receptor binding (DeNardo et al. 2009).

A phage-display method was used to discover a novel VAP-1 binding peptide. When further studies were conducted, this peptide revealed to belong to an unknown leukocyte ligand of VAP-1. This peptide was a part of a siglec-9 molecule that is found on granulocytes and macrophages. The combination of VAP-1 as a target and its natural binding structure as an imaging tool provides a theoretically optimal setting. Stabilizing the PEG spacer was incorporated into the peptide and it was labeled with ^{68}Ga. In Study III, we showed that in rodent models of inflammation and cancer that they could be detected by using a VAP-1 binding peptide labeled with ^{68}Ga, and that this binding was specific as confirmed with blocking studies with the cold peptide in the melanoma model. Autoradiography showed VAP-1 specific intratumoral binding of the peptide. VAP-1 positive transgenic mice showed a higher signal in chemically induced ear inflammation in comparison to the control site and to VAP-1 deficient knockout mice. The labeled peptide showed preferred renal excretion and some uptake in the liver.

In the last Study IV, we wanted to evaluate the whole-body distribution and pharmacokinetics of [^{124}I]BTT-1023 by the PET/CT imaging of healthy rabbits. [^{124}I]BTT-1023 showed VAP-1 specific binding after radioiodination, and this was confirmed by cell binding studies and digital autoradiography. The PET data was further used for

estimating the human radiation burden in prospective clinical trials with [^{124}I]BTT-1023. Previously, clinical PET imaging and dosimetry of several ^{124}I-labeled substances have been reported by other researchers. The injected ^{124}I radioactivities of 30–100 MBq have successfully revealed brain, lung, renal, thyroid, colorectal and breast tumors, as well as lymph node metastases (Wilson et al. 1991, Larson et al. 1992, Freuberg et al. 2004, Divgi et al. 2007, Farmakis et al. 2008, Jayson et al. 2009, Mumprecht et al. 2010, Carrasquillo et al. 2011, Tran et al. 2011). For example, Jayson and co-workers (Jayson et al. 2009) report that for 80 MBq of intravenously injected [^{124}I]HuMV833 antibody, the effective dose was 0.3 mSv/MBq when the thyroid uptake of radioiodine was blocked. In our case, even with successful thyroid blockage, the human radiation dose of [^{124}I]BTT-1023 (0.55±0.08 mSv/MBq) would still be approximately 30-fold higher than with [^{18}F]-FDG (0.019 mSv/MBq). The detection of [^{124}I]BTT-1023, for example, in an inflamed human joint, should be possible with an injected radioactivity of 0.5–0.7 MBq/kg, since there is less background activity, scatter and random activity in the vicinity. Moreover, a joint is reasonably easy to stabilize to minimize the effect of the object's movements on the signal quality. The final decision on the patient administration of [^{124}I]BTT-1023 depends on the expected benefits for the patient from this type of imaging study, for example, earlier diagnosis, confirmation of an appropriate treatment plan and more accurate follow up.

In addition to immuno-PET, also SPECT imaging with ^{123}I ($t_{1/2}$ 13.3 h) could be useful for patient imaging. An important benefit of replacing ^{124}I with, for example, ^{123}I, would be the lower radiation burden; the estimated effective dose for [^{123}I]BTT-1023 is 0.023 mSv/MBq when assuming a similar distribution pattern as for [^{124}I]BTT-1023 and the effective blocking of the thyroid glands. Since the results of the current study revealed that the clearance from blood circulation and the binding kinetic of [^{124}I]BTT-1023 to a highly VAP-1 positive liver is rather fast, studies with shorter lived radionuclides, such as ^{64}Cu ($t_{1/2}$ 12.7 h), ^{18}F ($t_{1/2}$ 109.8 min) and ^{68}Ga ($t_{1/2}$ 67.6 min) may be feasible. Indeed these radionuclides have been used for immuno-PET studies (Garg et al. 1991, Eder et al. 2010, Rossin et al. 2011).

6.5 LIMITATIONS IN VASCULAR ADHESION PROTEIN-1 IMAGING

VAP-1 binding peptides and antibodies have few limitations in PET imaging. For instance, all the tested imaging agents are too large or hydrophilic to cross the blood-brain-barrier, thus limiting their use in the imaging of diseases of the central nervous system. This could also be an interesting approach, since VAP-1 have been shown to play a role in animal models of several neurological diseases, such as EAE and ischemic brain stroke (Xu et al. 2006, O´Rourke et al. 2007).

The imaging of the abdomen area is also limited, since the liver shows high uptake. The liver uptake is, at least in part, due to the high number of VAP-1 receptors in the sinusoidal endothelial cells in the human liver (Lalor et al. 2002). Some degradation

products of [^{68}Ga]-DOTA-peptides, such as free ^{68}Ga, also tend to accumulate in the liver (Ujula et al. 2008). In studies with [^{68}Ga]-labeled siglec-9 peptide, blocking studies and a comparison of VAP-1 positive WT mice and VAP-1 negative KO mice, revealed 60 % and 47 % specific binding of the peptide in the liver, respectively. High uptake in the liver was also shown with [^{124}I]BTT-1023. In addition to VAP-1 specific binding, the hepatic uptake of antibodies might be caused by another mechanism, for example, metabolisms or binding to variants of neonatal receptors. To measure the degree of specific binding of the labelled antibody *in vivo*, blocking studies are going to be performed in the future. Although, earlier Jaakkola and co-workers demonstrated the uptake of a labeled antibody in the liver was partly VAP-1 specific in comparison to a non-specific antibody (Jaakkola et al. 2000).

VAP-1 has a soluble form in the circulation, secreted from the endothelial cell surface (Stolen et al 2005). The binding of labeled peptides to soluble VAP-1 might theoretically limit their use as an imaging target in cases in which the soluble VAP-1 concentrations are very high. In our studies, all inflammatory and cancer focuses were detectable from the background tissue, indicating that the soluble form is not a problem.

Also the excretion to the urine via the kidneys limits the use of these peptides in the imaging of the pelvic area. The antibody [^{124}I]BTT-1023 might be a more feasible imaging agent of the pelvic area, since only detached iodine is excreted via the urinary track. The antibody is most likely excreted via the hepatobiliary system. However, during the 4-day imaging schedule we did not observe any radioactivity in the gall bladder. High uptake of radioactivity in the thyroid glands was seen during the antibody imaging studies, which is most plausibly due to the release of ^{124}I from the antibody. Free iodine is rapidly taken up by thyroid glands and the excess is excreted via the kidneys to the urine.

6.6 FUTURE PROSPECTS

VAP-1 is upregulated in many inflammatory diseases, such as acute myocardial infarction, spontaneously developing insulitis in non-obese diabetic mice, and in animal models of RA and IBD (Salmi and Jalkanen 1992, Salmi et al. 1993, Salmi et al. 1997, Bono et al. 1999, Jaakkola et al 2000). In addition to these inflammatory diseases, also fatty liver and liver cirrhosis might be potential imaging targets. Leukocyte extravasation from the blood into inflamed tissues plays a crucial role in the pathogenesis of these diseases. The molecular imaging of adhesion molecules expressed on the vasculature of the target organs in these diseases could help in the diagnosis and evaluation of the severity of these diseases, as well as in the selection of patients for specific antibody treatment, monitoring these treatments and disease progression. This approach could also be utilized in VAP-1 specific drug development and the selection of patients for clinical trials.

In addition to inflammatory diseases, analyses of melanoma tumors have shown that vessels within the cancer express VAP-1 in humans (Forster-Horvath et al. 2004). Recently it has been discovered that VAP-1 activity enhances tumor angiogenesis and tumor growth in mice model of melanoma by increasing the recruitment of leukocytes into the tumors (Marttila-Ichihara et al. 2009). According to recent review by Ren and co-workers the imaging of melanoma would fasten the development of effective protocols for melanoma treatment (Ren et al. 2010). Thus, VAP-1 imaging might provide novel information about primary melanomas as well as the staging of metastasis. VAP-1 binding peptide/antibody could also be useful in receptor-targeted radiotherapy of melanoma. In addition to melanoma, also primary hepatocellular carcinomas, as well as squamous cell carcinoma of the head and neck, are known to express VAP-1 on their vasculature (Yoong et al. 1998, Irjala et al. 2001).

In addition to the molecular imaging of insulitis during the development of diabetes, the imaging of the pancreas is interesting for another reason. We showed that the vasculature in a pancreatic adenocarsinoma xenograft was VAP-1 negative, as well as lacking inflammatory cells in the tumor stroma. Because of this difference, *in vivo* imaging of VAP-1 could be feasible in the differential diagnostics of pancreatic adenocarsinoma and insulitis. The uptake in a normal pancreas, at least for [^{68}Ga]-DOTAVAP-P1, was very low, suggesting that the imaging of the pancreas might be a feasible option (Ujula et al. 2009).

Although VAP-1 imaging provides a lot of possibilities, several hurdles need to be overcome before this approach can be fully exploited. For instance, in the case of the peptides, the specific radioactivity should be improved. Also, further preclinical testing should be performed with several animal models to validate the feasibility of the peptides in imaging. To evaluate the potential of these VAP-1 targeting peptides in a clinical setting, dosimetry evaluation needs to be performed on animals. In order to apply the therapy aspect with the peptides, internalization should be confirmed. In the case of a labeled antibody, the targeting of VAP-1 in an animal model of the disease and the effective blocking of released iodine has to be confirmed. All these studies are proof-of-concept studies and further studies are warranted.

7 CONCLUSIONS

During this work, the preclinical evaluation of several VAP-1 targeting PET imaging agents was performed. The first study evaluated the first-in-line peptide, GGGGKGGGG, targeting VAP-1. Studies showed that the [^{68}Ga]-DOTA labeled peptide was able to delineate acute, sterile inflammation comparable with [^{18}F]-FDG, the golden standard in PET imaging. In addition, the tumor uptake of [^{68}Ga]-DOTAVAP-P1 was low in contrast to prominent [^{18}F]-FDG uptake. These results are in line with the luminal expression of VAP-1 on the vasculature in these experimental models.

Even though [^{68}Ga]-DOTAVAP-P1 showed promising qualities for the PET imaging of inflammation, we wanted to further study whether the imaging quality could be improved with the incorporation of a mini-PEG spacer. This approach showed enhanced *in vivo* stability leading to higher target-to-background ratios and improved *in vivo* PET imaging of experimental inflammation.

Phage display enables a fast screening of specific binding peptides. The approach led to the discovery of siglec-9, a novel ligand for VAP-1. We were able to show that a combination of VAP-1 as a target and its natural binding structure as an imaging tool provides, theoretically, an optimal setting for imaging inflammation and the inflammatory component of some cancers, such as melanoma. In this work, we showed the proof of concept for this idea, and further studies will test its usability in patients.

In addition to [^{68}Ga]-labeled peptides, the capacity of VAP-1 binding antibody, BTT-1023, was tested in PET imaging after radioiodination. [^{124}I]BTT-1023 was able to bind to VAP-1, both *in vitro* and *in vivo* settings, and further elucidated the whole-body distribution and kinetics of fully human anti-VAP-1antibody over the time period of 4 days. Since the radiation burden of ^{124}I labeled antibody is rather high, another isotope might be more feasible for the labelling procedure. Further studies are warranted to clarify the fate of these imaging agents in animal models of inflammation and cancer and clinical settings.

8 ACKNOWLEDGEMENTS

This study was carried out in the Turku PET Centre, Institute of Clinical Medicine, Department of Clinical Physiology and Nuclear Medicine during the years 2007-2011. Professor Juhani Knuuti, the director of the Turku PET Centre and Professor Jaakko Hartiala, the head of the Department of Clinical Physiology and Nuclear Medicine, are warmly acknowledged for allowing me to use their facilities during this study.

I owe my deepest gratitude to my supervisors, Professor Anne Roivainen and Professor Sirpa Jalkanen. Anne is thanked for her support and encouragement during these years. Her trust in me and in our research has been the carrying force during these studies. Sirpa is thanked for always having time to go through data as well as manuscripts with me. Having such a dynamic duo as supervisors has been a privilege for me. Both of you have inspired me with your never ending passion for science. I want to also thank Professor Mika Scheinin, the director of the FinPharma Doctoral Program Drug Discovery Section, (previously known as DDGS), Dr. Eeva Valve, the coordinator of the program, as well as the whole graduate school for all the support they have provided for me. Thanks to the personnel of BioTie Therapies and MAP Medicals. Especially Dr. Petri Vainio, Dr. Jani Vainio from BioTie, as well as Antti Mali from MAP Medicals, are acknowledged. I would also like to thank all the other co-authors of the original publications. Furthermore, my supervisory board members, Anne, Sirpa and Professor Markku Koulu and Professor Pirjo Nuutila, are gratefully acknowledged. Sincere thanks to Professor Juhani Knuuti and Professor Pirjo Nuutila for including me in the activities of the Centre of Excellence in Molecular Imaging in Cardiovascular and Metabolic Research.

My gratitude goes to all of the personnel in PET Centre. I am grateful for all the discussions and laughter we have shared in the coffee room and even though all of you are not mentioned here, you are warmly thanked for always being willing to help me and providing such a fun and inspiring atmosphere to work in. The lovely ladies in lab (Sanna Suominen, Heidi Partanen, Eija Nirhamo and Emilia Puhakka) are thanked for their help and advices as well as Tarja Keskitalo and Minna Aatsinki for their help with scheduling and camera reservations. Leena Tokoi-Eklund is acknowledged for her expertise with animal imaging. Sami Suilamo, Jarkko Johansson, Mika Teräs, Tuula Tolvanen and Marko Tirri are thanked for their help with all cameras, reconstructions and with all the physics and mathematics related matters. Pauliina Luoto, Henri Sipilä, Tiina Saanijoki and Satu Salomäki are acknowledged for ^{68}Ga-labeling and their expertise with radioHPLC. Vesa Oikonen is acknowledged for his assistance with modelling and biokinetics as well as Marko Tättäläinen and Rami Mikkola, for help with information technology. All the members in the CoE are acknowledged for interesting discussions of life and science during these years. I am grateful for Iina, Pauliina, Tiina, Johanna, Tipi, Tommi, Jarkko, Henkka, Gaber and Marco as well as Nikke and Ralu for being friends when I needed one. I wish to thank all the members in Anne's group. In particular I am thankful for my sisters in science, Iina and Tiina for teaching me all the practical matters. Also Anne`s Angels are acknowledged for being such a splendid travelling companions in all the congress trips.

I wish to also thank Sirpa's group. I am grateful for all the help you have provided as well as all the scientific discussions to improve our manuscripts. Sari Mäki is thanked for

immunohistochemical staining and Riikka Sjöroos for culturing the cells. In particular I am thankful for Kristiina Aalto and Mikael Maksimow for their help and advices. I thank for Anu Airaksinen and Aapo Ahonen for their excellent comments during reviewing process of this thesis. I thank Henno Parks for reviewing the language and Timo Kattelus for processing the images. I want to thank Jouko Sandholm for his help with microscope and images and all the personnel of the Central Animal Laboratory, particularly Rafael Frias. Also the personnel of Turku Center for Disease Modeling are thanked, Erja Mäntysalo and Nina Messner for their assistance during animal imaging studies and Erica Nyman for tissue sectioning and stainings as well as Tarja Lamminen for the cell culturing. Tero Karhi is acknowledged for his excellent ideas concerning study setup. For secretarial matters, Mirja Jyrkinen, Laura Jaakkola and Sinikka Lehtola from the PET Centre, as well as Anne Sovikoski-Georgieva from MediCity are acknowledged.

Furthermore, I want to thank our class in Health Biosciences ’03 and Professors Markku Koulu, Liisa Kanerva, Sari Mäkelä and Seppo Salminen. Also students in DDGS, especially Mirkka, Heli and Päivi, are thanked for being excellent company during many national and international congresses. I wish to thank my dear friends for their support, especially the sopulit Anniina, Karo, Minna, Taina and Tuija for giving me something else to think about besides work. I wish to thank you for your friendship throughout all of these years. Pauliina and Iina are thanked for making every day in work more fun, for jogging and sauna companion and always being there for me.

My parents-in-law Pirjo and Markku Koskinen as well as my sister-in-laws, Outi and Paula with her family, are thanked for their support and for providing essential help. My mother Raisa and my father Osmo Autio as well as my brother Teemu are thanked for their love and support. All of my grandparents are thanked for teaching me the valuable lesson of the power of will and hard work. In addition, Raisa and Pirjo are thanked for taking such an excellent care of our baby boy and leaving my mind free to worry other things. Our one-year-old son, Jami, is thanked for making me smile and for teaching me something my mother and husband have tried to teach me in vain, patience. My husband Mikko, without your help, my thesis would still be a combination of unopened data files; email attachments sent to oblivion and destroyed excel and word documents. In addition to technical help, you have been the most demanding critic with your need to find an application to every new scientific finding. Thank you for providing me with a fresh point of view every now and then. Thank you for always believing in me.

This study was financially supported by grants from the EVO-grants of the Hospital District of Southwest Finland, the Finnish Cultural Foundation, the Instrumentarium Foundation and the FinPharma Doctoral Program Drug Discovery Section. The study was conducted within the Finnish Centre of Excellence in Molecular Imaging in Cardiovascular and Metabolic Research supported by the Academy of Finland, University of Turku, Turku University Hospital and Åbo Akademi University.

Turku, February 2012

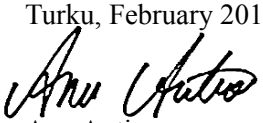

Anu Autio

9 REFERENCES

Abella A., García-Vicente S., Viguerie N., Ros-Baró A., Camps M., Palacín M., Zorzano A., Marti L. (2004). Adipocytes release a soluble form of VAP-1/SSAO by a metalloprotease-dependent process and in a regulated manner. *Diabetologia* **47**, 429-438.

Airenne T.T., Nymalm Y., Kidron H., Smith D.J., Pihlavisto M., Salmi M., Jalkanen S., Johnson M.S., Salminen T.A. (2005). Crystal structure of the human vascular adhesion protein-1: unique structural features with functional implications. *Protein Sci* **14**, 1964-1974.

Akizawa H., Uehara T., Arano Y. (2008). Renal uptake and metabolism of radiopharmaceuticals derived from peptides and proteins. *Adv Drug Deliv Rev* **60**, 1319-1328.

Aspinall A.I., Curbishley S.M., Lalor P.F., Weston C.J., Blahova M., Liaskou E., Adams R.M., Holt A.P., Adams D.H. (2010). CX(3)CR1 and vascular adhesion protein-1-dependent recruitment of CD16(+) monocytes across human liver sinusoidal endothelium. *Hepatology* **51**, 2030-2039.

Balkwill F. and Mantovani A. (2001). Inflammation and cancer: back to Virchow? *Lancet* **35**, 7539-7545.

Balkwill F. and Coussens L.M. (2004). Cancer: an inflammatory link. *Nature* **431**, 405-406.

Beer A.J., Haubner R., Sarbia M., Goebel M., Luderschmidt S., Grosu A.L., Schnell O., Niemeyer M., Kessler H., Wester H.J., Weber W.A., Schwaiger M. (2006). Positron emission tomography using [^{18}F]Galacto-RGD identifies the level of integrin alpha(v)beta3 expression in man. *Clin Cancer Res* **12**, 3942-3949.

Beer A.J. and Schwaiger M. (2008). Imaging of integrin alphavbeta3 expression. *Cancer Metastasis Rev* **27**, 631-644.

Bhatti M., Chapman P., Peters M., Haskard D., Hodgson H.J. (1998). Visualising E-selectin in the detection and evaluation of inflammatory bowel disease. *Gut* **43**, 40-47.

Boerman O.C., Rennen H., Oyen W.J., Corstens F.H. (2001). Radiopharmaceuticals to image infection and inflammation. *Semin Nucl Med* **31**, 286-295.

Boerman O.C. and Oyen W.J. (2011). Immuno-PET of cancer: a revival of antibody imaging. *J Nucl Med* **52**, 1171-1172.

Bonder C.S., Norman M.U., Swain M.G., Zbytnuik L.D., Yamanouchi J., Santamaria P., Ajuebor M., Salmi M., Jalkanen S., Kubes P. (2005). Rules of recruitment for Th1 and Th2 lymphocytes in inflamed liver: a role for alpha-4 integrin and vascular adhesion protein-1. *Immunity* **23**, 153-163.

Bono P., Jalkanen S., Salmi M. (1999). Mouse vascular adhesion protein 1 is a sialoglycoprotein with enzymatic activity and is induced in diabetic insulitis. *Am J Pathol* **155**, 1613-1624.

Boomsma F., Bhaggoe U.M., van der Houwen A.M., van den Meiracker A.H. (2003). Plasma semicarbazide-sensitive amine oxidase in human (patho)physiology. *Biochim Biophys Acta* **1647**, 48-54.

Boomsma F., Hut H., Bagghoe U., van der Houwen A., van den Meiracker A. (2005). Semicarbazide-sensitive amine oxidase (SSAO): from cell to circulation. *Med Sci Monit* **11**, 122-126.

Broisat A., Riou L.M., Ardisson V., Boturyn D., Dumy P., Fagret D., Ghezzi C. (2007). Molecular imaging of vascular cell adhesion molecule-1 expression in experimental atherosclerotic plaques with radiolabelled B2702-p. *Eur J Nucl Med Mol Imaging* **34**, 830-840.

Butcher E.C. (1992). Leukocyte-endothelial cell adhesion as an active, multi-step process: a combinatorial mechanism for specificity and diversity in leukocyte targeting. *Adv Exp Med Biol* **323**, 181-194.

Butcher E.C. and Picker L.J. (1996). Lymphocyte homing and homeostasis. *Science* **272**, 60-66.

Björke H. and Andersson K. (2006). Automated, high-resolution cellular retention and uptake studies in vitro. *Appl Radiat Isot* **64**, 901–905.

Cai W., Gambhir S.S., Chen X. (2005). Multimodality tumor imaging targeting integrin alpha$_v$beta$_3$. *Biotechniques* **39**, S14-25.

Cao Q., Cai W., Li Z.B., Chen K., He L., Li H.C., Hui M., Chen X. (2007). PET imaging of acute and

chronic inflammation in living mice. *Eur J Nucl Med Mol Imaging* **34**, 1832-1842.

Carrasquillo J.A., Pandit-Taskar N., O'Donoghue J.A., Humm J.L., Zanzonico P., Smith-Jones P.M., Divgi C.R., Pryma D.A., Ruan S., Kemeny N.E., Fong Y., Wong D., Jaggi J.S., Scheinberg D.A., Gonen M., Panageas K.S., Ritter G., Jungbluth A.A., Old L.J., Larson S.M. (2011). ^{124}I-huA33 antibody PET of colorectal cancer. *J Nucl Med* **52**, 173–180.

Chapman P.T., Jamar F., Harrison A.A., Schofield J.B., Peters A.M., Binns R.M., Haskard D.O. (1996a). Characterization of E-selectin expression, leucocyte traffic and clinical sequelae in urate crystal-induced inflammation: an insight into gout. *Br J Rheumatol* **35**, 323-334.

Chapman P.T., Jamar F., Keelan E.T., Peters A.M., Haskard D.O. (1996b). Use of a radiolabeled monoclonal antibody against E-selectin for imaging of endothelial activation in rheumatoid arthritis. *Arthritis Rheum* **39**, 1371-1375.

Chen K. and Conti P.S. (2010). Target-specific delivery of peptide-based probes for PET imaging. *Adv Drug Deliv* Rev **62**, 1005-1022.

Chen X., Park R., Shahinian A.H., Bading J.R., Conti P.S. (2004a). Pharmacokinetics and tumor retention of ^{125}I-labeled RGD peptide are improved by PEGylation. *Nucl Med Biol* **31**, 11-19.

Chen X., Hou Y., Tohme M., Park R., Khankaldyyan V., Gonzales-Gomez I., Bading J.R., Laug W.E., Conti P.S. (2004b). Pegylated Arg-Gly-Asp peptide: ^{64}Cu labeling and PET imaging of brain tumor alpha$_v$beta$_3$-integrin expression. *J Nucl Med* **45**, 1776-1783.

Cheng D., Wang Y., Liu X., Pretorius H., Liang M., Rusckowski M., Hnatowich D.J. (2010). A comparison of ^{18}F PET and ^{99m}Tc SPECT imaging in phantoms and in tumored mice. *Bioconjug Chem* **21**, 1565-1570.

Coussens L.M. and Werb Z. (2002). Inflammation and cancer. *Nature* **420**, 860-867.

Crocker P.R., Paulson J.C., Varki A. (2007). Siglecs and their roles in the immune system. *Nat Rev Immunol* **7**, 255-266.

DeNardo S.J., Liu R., Albrecht H., Natarajan A., Sutcliffe J.L., Anderson C., Peng L., Ferdani R., Cherry S.R., Lam K.S. (2009). ^{111}In-LLP2A-DOTA polyethylene glycol targeting a$_4$b$_1$ integrin: comparative pharmacokinetics for imaging and therapy of lymphoid malignancies. *J Nucl Med* **50**, 625-634.

Dijkgraaf I., Yim C.B., Franssen G.M., Schuit R.C., Luurtsema G., Liu S., Oyen W.J., Boerman O.C. (2011). PET imaging of $\alpha^v\beta^3$ integrin expression in tumours with ^{68}Ga-labelled mono-, di- and tetrameric RGD peptides. *Eur J Nucl Med Mol Imaging* **38**, 128-137.

Divgi C.R., Pandit-Taskar N., Jungbluth A.A., Reuter V.E., Gönen M., Ruan S., Pierre C., Nagel A., Pryma D.A., Humm J., Larson S.M., Old L.J., Russo P.l. (2007). Preoperative characterisation of clear-cell renal carcinoma using iodine-124-labelled antibody chimeric G250 (^{124}I-cG250) and PET in patients with renal masses: a phase I trial. *Lancet Oncol* **8**, 304–310.

van Dongen G.A. and Vosjan M.J. (2010). Immuno-positron emission tomography: shedding light on clinical antibody therapy. *Cancer Biother Radiopharm* **25**, 375-385.

Dunkel P., Gelain A., Barlocco D., Haider N., Gyires K., Sperlágh B., Magyar K., Maccioni E., Fadda A., Mátyus P. (2008). Semicarbazide-sensitive amine oxidase/vascular adhesion protein 1: recent developments concerning substrates and inhibitors of a promising therapeutic target. *Curr Med Chem* **15**, 1827-1839.

Eder M., Knackmuss S., Le Gall F., Reusch U., Rybin V., Little M., Haberkorn U., Mier W., Eisenhut M. (2010). ^{68}Ga-labelled recombinant antibody variants for immuno-PET imaging of solid tumours. *Eur J Nucl Med Mol Imaging* **37**, 1397–407.

Farmakis G., Brandau W., Hellwig D., Wollenweber F., Schaefer A., Kirsch C.M., Samnick S. (2008). PET imaging with p-[I-124]iodo-l-phenylalanine as a new tool for diagnosis and postoperative control in patients with glioma. *Clin Nucl Med* **33**, 441–442.

Forster-Horváth C., Döme B., Paku S., Ladányi A., Somlai B., Jalkanen S., Tímár J. (2004). Loss of vascular adhesion protein-1 expression in intratumoral microvessels of human skin melanoma. *Melanoma Res* **14**, 135-140.

Freudenberg L.S., Antoch G., Jentzen W., Pink R., Knust J., Görges R., Müller S.P., Bockisch A., Debatin J.F., Brandau W. (2004). Value of 124-IPET/CT in staging of patients with differential thyroid cancer. *Eur Radiol* **14**, 2092–2098.

Garg P.K., Garg S., Zalutsky M.R. (1991). Fluorine-18 labeling of monoclonal antibodies and fragments with preservation of immunoreactivity. *Bioconjugate Chem* **2**, 44–49.

Gotthardt M., Boermann O.C., Behr T.M., Béhé M.P., Oyen W.J. (2004). Development and clinical application of peptide-based radiopharmaceuticals. *Curr Pharm Des* **10**, 2951-2963.

Gotthardt M., Bleeker-Rovers C.P., Boerman O.C., Oyen W.J. (2010). Imaging of inflammation by PET, conventional scintigraphy, and other imaging techniques. *J Nucl Med* **51**, 1937-1949.

Göktürk C., Garpenstrand H., Nilsson J., Nordquist J., Oreland L., Forsberg-Nilsson K. (2003). Studies on semicarbazide-sensitive amine oxidase in patients with diabetes mellitus and in transgenic mice. *Biochim Biophys Acta* **1647**, 88-91.

Haubner R., Wester H.J., Reuning U., Senekowitsch-Schmidtke R., Diefenbach B., Kessler H., Stöcklin G., Schwaiger M. (1999). Radiolabeled alpha(v) beta3 integrin antagonists: a new class of tracers for tumor targeting. *J Nucl Med* **40**, 1061-71.

Haubner R., Wester H.J., Weber W.A., Mang C., Ziegler S.I., Goodman S.L., Senekowitsch-Schmidtke R., Kessler H., Schwaiger M. (2001). Noninvasive imaging of alpha(v)beta3 integrin expression using ^{18}F-labeled RGD-containing glycopeptide and positron emission tomography. *Cancer Res* **61**, 1781-1785.

Haubner R., Kuhnast B., Mang C., Weber W.A., Kessler H., Wester H.J., Schweiger M. (2004). [^{18}F] Galacto-RGD: synthesis, radiolabeling, metabolic stability and radiation dose estimates. *Bioconjugate Chem* **15**, 61-69.

Haubner R., Weber W.A., Beer A.J., Vabuliene E., Reim D., Sarbia M., Becker K.F., Goebel M., Hein R., Wester H.J., Kessler H., Schwaiger M. (2005). Noninvasive visualization of the activated alphavbeta3 integrin in cancer patients by positron emission tomography and [^{18}F]Galacto-RGD. *PLoS Med* **2**, e70.

Haubner R. (2006). Alphavbeta3-integrin imaging: a new approach to characterise angiogenesis? *Eur J Nucl Med Mol Imaging* **33**, Suppl 54-63.

Haukkala J., Laitinen I., Luoto P., Iveson P., Wilson I., Karlsen H., Cuthbertson A., Laine J., Leppänen P., Ylä-Herttula S., Knuuti J., Roivainen A. (2009). ^{68}Ga-DOTA-RGD peptide: biodistribution and binding into atherosclerotic plaques in mice. *Eur J Nucl Med Mol Imaging* **36**, 2058-2067.

Hamacher K**.**, Coenen H**.H.**, Stöcklin G. **(1986).** Efficient stereospecific synthesis of no-carrier-added 2-[18F]-fluoro-2-deoxy-D-glucose using aminopolyether supported nucleophilic substitution. *J Nucl Med* **27**, 235-238.

Irjala H., Salmi M., Alanen K., Grénman R., Jalkanen S. (2001). Vascular adhesion protein 1 mediates binding of immunotherapeutic effector cells to tumor endothelium. *J Immunol* **166**, 6937-6943.

Jaakkola K., Nikula T., Holopainen R., Vähäsilta T., Matikainen M.T., Laukkanen M.L., Huupponen R., Halkola L., Nieminen L., Hiltunen J., Parviainen S., Clark M.R., Knuuti J., Savunen T., Kääpä P., Voipio-Pulkki L.M., Jalkanen S. (2000a). In vivo detection of vascular adhesion protein-1 in experimental inflammation. *Am J Pathol* **157**, 463-471.

Jaakkola K., Jalkanen S., Kaunismäki K., Vänttinen E., Saukko P., Alanen K., Kallajoki M., Voipio-Pulkki L.M., Salmi M. (2000b). Vascular adhesion protein-1, intercellular adhesion molecule-1 and P-selectin mediate leukocyte binding to ischemic heart in humans. *J Am Coll Cardiol* **36**, 122-129.

Jamar F., Houssiau F.A., Devogelaer J.P., Chapman P.T., Haskard D.O., Beaujean V., Beckers C., Manicourt D.H., Peters A.M. (2002). Scintigraphy using a technetium 99m-labelled anti-E-selectin Fab fragment in rheumatoid arthritis. *Rheumatology* **41**, 53-61.

Jayson G., Zweit J., Jackson A., Mulatero C., Julyan P., Ranson M., Broughton .L, Wagstaff J., Hakannson L., Groenewegen G., Bailey J., Smith N., Hastings D., Lawrance J., Haroon H., Ward T., McGown A.T., Tang M., Levitt D., Marreaud S., Lehmann F.F., Herold M., Zwierzina H. (2002). Molecular imaging and biological evaluation of HuMV833 anti-VEGF antibody: implications for trial design of antiangiogenic antibodies. *J Natl Cancer Inst* **94**, 1484–1493.

Ji S., Fang W., Zhu M., Bai X., Wang C., Ruan C. (2011). Detection of pulmonary embolism with 99mTc-labeled F(ab)2 fragment of anti-P-selectin monoclonal antibody in dogs. *Tohoku J Exp Med* **223**, 9-15.

de Jong H.W., van Velden F.H., Kloet R.W., Buijs F.L., Boellaard R., Lammertsma A.A. (2007) Performance evaluation of the ECAT HRRT: an

LSO-LYSO double layer high resolution, high sensitivity scanner. *Phys Med Biol* **52**, 1505-1526.

Ke S., Wen X., Wu Q.P., Wallace S., Charnsangavej C., Stachowiak A.M., Stephens C.L., Abbruzzese J.L., Podoloff D.A., Li C. (2004). Imaging taxane-induced tumor apoptosis using PEGylated, ^{111}In-labeled annexin V. *J Nucl Med* **45**, 108-115.

Keelan E.T., Harrison A.A., Chapman P.T., Binns R.M., Peters A.M., Haskard D.O. (1994). Imaging vascular endothelial activation: an approach using radiolabeled monoclonal antibodies against the endothelial cell adhesion molecule E-selectin. *J Nucl Med* **35**, 276-281.

Kiss J., Jalkanen S., Fülöp F., Savunen T., Salmi M. (2008). Ischemia-reperfusion injury is attenuated in VAP-1-deficient mice and by VAP-1 inhibitors. *Eur J Immunol* **38**, 3041-3049.

Kivi E., Elima K., Aalto K., Nymalm Y., Auvinen K., Koivunen E., Otto D.M., Crocker P.R., Salminen T.A., Salmi M., Jalkanen S. (2009). Human Siglec-10 can bind to vascular adhesion protein-1 and serves as its substrate. *Blood* **114**, 5385-5392.

Koskinen K., Vainio P.J., Smith D.J., Pihlavisto M., Ylä-Herttuala S., Jalkanen S., Salmi M. (2004). Granulocyte transmigration through the endothelium is regulated by the oxidase activity of vascular adhesion protein-1 (VAP-1). *Blood* **103**, 3388-3395.

Koskinen K., Nevalainen S., Karikoski M., Hänninen A., Jalkanen S., Salmi M. (2007). VAP-1-deficient mice display defects in mucosal immunity and antimicrobial responses: implications for antiadhesive applications. *J Immunol* **179**, 6160-6168.

Kurkijärvi R., Yegutkin G.G., Gunson B.K., Jalkanen S., Salmi M., Adams D.H. (2000). Circulating soluble vascular adhesion protein 1 accounts for the increased serum monoamine oxidase activity in chronic liver disease. *Gastroenterology* **119**, 1096-1103.

Kurkijärvi R., Jalkanen S., Isoniemi H., Salmi M. (2001). Vascular adhesion protein-1 (VAP-1) mediates lymphocyte-endothelial interactions in chronic kidney rejection. *Eur J Immunol* **31**, 2876-2884.

Laitinen I., Saraste A., Weidl E., Poethko T., Weber A.W., Nekolla S.G., Leppänen P., Ylä-Herttuala S., Hölzlwimmer G., Walch A., Esposito I., Wester H.J., Knuuti J., Schwaiger M. (2009). Evaluation of alphavbeta3 integrin-targeted positron emission tomography tracer ^{18}F-galacto-RGD for imaging of vascular inflammation in atherosclerotic mice. *Circ Cardiovasc Imaging* **2**, 331-338.

Lalor P.F., Edwards S., McNab G., Salmi M., Jalkanen S., Adams D.H. (2002). Vascular adhesion protein-1 mediates adhesion and transmigration of lymphocytes on human hepatic endothelial cells. *J Immunol* **169**, 983-992.

Lalor P.F., Sun P.J., Weston C.J., Martin-Santos A., Wakelam M.J., Adams D.H. (2007). Activation of vascular adhesion protein-1 on liver endothelium results in an NF-kappaB-dependent increase in lymphocyte adhesion. *Hepatology* **45**, 465-474.

Lankinen P., Mäkinen T.J., Pöyhönen T.A., Virsu P., Salomäki S., Hakanen A.J., Jalkanen S., Aro H.T., Roivainen A. (2008). (68)Ga-DOTAVAP-P1 PET imaging capable of demonstrating the phase of inflammation in healing bones and the progress of infection in osteomyelitic bones. *Eur J Nucl Med Mol Imaging* **35**, 352-364.

Larson S.M., Pentlow K.S., Volkow N.D., Wolf A.P., Finn R.D., Lambrecht R.M., Graham M.C., Di Resta G., Bendnem B., Daghighian F., Yeh S.D.J., Wang G.-J., Cheung N-K.V. (1992). PET scanning of iodine-124-3F9 as an approach to tumor dosimetry during treatment planning for radioimmunotherapy in a child with neuroblastoma. *J Nucl Med* **33**, 2020–2023.

Lee S., Xie J., Chen X. (2010). Peptide-based probes for targeted molecular imaging. *Biochemistry* **49**, 1364-1376.

Ley K. and Kansas G.S. (2004). Selectins in T-cell recruitment to non-lymphoid tissues and sites of inflammation. *Nat Rev Immun*ol **4**, 325-335.

Ley K., Laudanna C., Cybulsky M.I., Nourshargh S. (2007). Getting to the site of inflammation: the leukocyte adhesion cascade updated. *Nat Rev Immunol* **7**, 678-689.

Liaskou E., Karikoski M., Reynolds G.M., Lalor P.F., Weston C.J., Pullen N., Salmi M., Jalkanen S., Adams D.H. (2011). Regulation of mucosal addressin cell adhesion molecule 1 expression in human and mice by vascular adhesion protein 1 amine oxidase activity. *Hepatology* **53**, 661-672.

Liu Z., Liu S., Wang F., Liu S., Chen X. (2009a). Noninvasive imaging of tumor integrin expression

using ^{18}F-labeled RGD dimer peptide with PEG_4 linkers. *Eur J Nucl Med Mol Imaging* **36**, 1296-1307.

Liu Z., Niu G., Shi J., Liu S., Wang F., Liu S., Chen X. (2009b). ^{68}Ga-labeled cyclic RGD dimers with Gly_3 and PEG_4 linkers: promising agents for tumor integrin $\alpha_v\beta_3$ PET imaging. *Eur J Nucl Med Mol Imaging* **36**, 947-957.

Love C., Tomas M.B., Tronco G.G., Palestro C.J. (2005). FDG PET of infection and inflammation. *Radiographics* **25**, 1357-1368.

Luster A.D., Alon R., von Andrian U.H. (2005). Immune cell migration in inflammation: present and future therapeutic targets. *Nat Immunol* **6**, 1182-1190.

Lyles G.A. (1996). Mammalian plasma and tissue-bound semicarbazide-sensitive amine oxidases: biochemical, pharmacological and toxicological aspects. *Int J Biochem Cell Biol* **28**, 259-274.

Mantovani A. (2005). Inflammation by remote control. *Nature* **435**, 752-753.

Mantovani A., Allavena .P, Sica A., Balkwill F. (2008). Cancer-related inflammation. *Nature* **454**, 436-444.

Martelius T., Salaspuro V., Salmi M., Krogerus L., Höckerstedt K., Jalkanen S., Lautenschlager I. (2004). Blockade of vascular adhesion protein-1 inhibits lymphocyte infiltration in rat liver allograft rejection. *Am J Pathol* **165**, 1993-2001.

Marttila-Ichihara F., Smith D.J., Stolen C., Yegutkin G.G., Elima K., Mercier N., Kiviranta R., Pihlavisto M., Alaranta S., Pentikäinen U., Pentikäinen O., Fülöp F., Jalkanen S., Salmi M. (2006). Vascular amine oxidases are needed for leukocyte extravasation into inflamed joints in vivo. *Arthritis Rheum* **54**, 2852-2862.

Marttila-Ichihara F., Auvinen K., Elima K., Jalkanen S., Salmi M. (2009). Vascular adhesion protein-1 enhances tumor growth by supporting recruitment of Gr-1+CD11b+ myeloid cells into tumors. *Cancer Res* **69**, 7875-7883.

Marttila-Ichihara F., Castermans K., Auvinen K., Oude Egbrink M.G., Jalkanen S., Griffioen A.W., Salmi M. (2010). Small-molecule inhibitors of vascular adhesion protein-1 reduce the accumulation of myeloid cells into tumors and attenuate tumor growth in mice. *J Immunol* **184**, 3164-3173.

McNab G., Reeves J.L., Salmi M., Hubscher S., Jalkanen S., Adams D.H. (1996). Vascular adhesion protein 1 mediates binding of T cells to human hepatic endothelium. *Gastroenterology* **110**, 522-528.

Medzhitov R. (2008). Origin and physiological roles of inflammation. *Nature* **454**, 428-435.

Merinen M., Irjala H., Salmi M., Jaakkola I., Hänninen A., Jalkanen S. (2005). Vascular adhesion protein-1 is involved in both acute and chronic inflammation in the mouse. *Am J Pathol* **166**,793-800.

Mumprecht V., Honer M., Vigl B., Proulx S.T., Trachsel E., Kaspar M., Banziger-Tobler N.E., Schibli R., Neri D., Detmar M. (2010). In vivo imaging of inflammation- and tumor-induced lymph node lymphangiogenesis by immuno-positron emission tomography. *Cancer Res* **70**, 8842–8851.

Mäcke H.R., Hofmann M.D., Haberkorn U. (2005). ^{68}Ga-labeled peptides in tumor imaging. *J Nucl Med* **46**, S172-178.

Nahrendorf M., Keliher E., Panizzi P., Zhang H., Hembrador S., Figueiredo J.L., Aikawa E., Kelly K., Libby P., Weissleder R. (2009). ^{18}F-4V for PET-CT imaging of VCAM-1 expression in atherosclerosis. *JACC Cardiovasc Imaging* **2**, 1213-22.

Nathan C. (2002). Points of control in inflammation. *Nature* **420**, 846-52.

Nikula T.K., Bocchia M., Curcio M.J., Sgouros G., Ma Y., Finn R.D., Scheinberg D.A. (1995) Impact of the high tyrosine fraction in complementarity determining regions: measured and predicted effects of radioiodination on IgG immunoreactivity. *Mol Immunol* **32,** 865-872.

Nikula T.K., McDevitt M.R., Finn R.D., Wu C., Kozak R.W., Garmestani K., Brechbiel M.W., Curcio M.J., Pippin C.G., Tiffany-Jones L., Geerlings M.W. Sr., Apostolidis C., Molinet R., Geerlings M.W. Jr., Gansow O.A., Scheinberg D.A. (1999). Alpha-emitting bismuth cyclohexylbenzyl DTPA constructs of recombinant humanized anti-CD33 antibodies: pharmacokinetics, bioactivity, toxicity and chemistry. *J Nucl Med* **40**, 166-176.

O'Rourke A.M., Wang E.Y., Salter-Cid L., Huang .L, Miller A., Podar E., Gao H.F., Jones D.S., Linnik M.D. (2007). Benefit of inhibiting SSAO in relapsing experimental autoimmune encephalomyelitis. *J Neural Transm* **114**, 845-849.

O'Rourke A.M., Wang E.Y., Miller A., Podar E.M., Scheyhing K., Huang L., Kessler C., Gao H., Ton-Nu H.T., Macdonald M.T., Jones D.S., Linnik M.D. (2008). Anti-inflammatory effects of LJP 1586 [Z-3-fluoro-2-(4-methoxybenzyl)allylamine hydrochloride], an amine-based inhibitor of semicarbazide-sensitive amine oxidase activity. *J Pharmacol Exp Ther* **324**, 867-875.

Pichler B.J., Kneilling M., Haubner R., Braumüller H., Schwaiger M., Röcken M., Weber W.A. (2005). Imaging of delayed-type hypersensitivity reaction by PET and ^{18}F-galacto-RGD. *J Nucl Med* **46**, 184-189.

Rahmim A. and Zaidi H. (2008). PET versus SPECT: strengths, limitations and challenges. *Nucl Med Commun* **29**, 193-207.

Ren G., Pan Y., Cheng Z. (2010). Molecular probes for malignant melanoma imaging. *Curr Pharm Biotechnol* **11**, 590-602.

Reubi J.C. and Mäcke H.R. (2008). Peptide-based probes for cancer imaging. *J Nucl Med* **49**, 1735-1738.

Rossin R., Kohno T., Hagooly A., Sharp T., Gliniak B., Arroll T., Chen Q., Hewig A., Kaplan-Lefko P., Friberg G., Radinsky R., Evelhoch J.L., Welch M.J., Hwang D.R. (2011). Characterization of ^{64}Cu-DOTA conatumumab: a PET tracer for in vivo imaging of death receptor 5. *J Nucl Med* **52**, 942–949.

Sackstein R. (2005). The lymphocyte homing receptors: gatekeepers of the multistep paradigm. *Curr Opin Hematol* **12**, 444-450.

Salmi M. and Jalkanen S. (1992). A 90-kilodalton endothelial cell molecule mediating lymphocyte binding in humans. *Science* **257**, 1407-1409.

Salmi M., Kalimo K., Jalkanen S. (1993). Induction and function of vascular adhesion protein-1 at sites of inflammation. *J Exp Med* **178**, 2255-2260.

Salmi M. and Jalkanen S. (1996). Human vascular adhesion protein 1 (VAP-1) is a unique sialoglycoprotein that mediates carbohydrate-dependent binding of lymphocytes to endothelial cells. *J Exp Med* **183**, 569-79.

Salmi M., Rajala P., Jalkanen S. (1997). Homing of mucosal leukocytes to joints. Distinct endothelial ligands in synovium mediate leukocyte-subtype specific adhesion. *J Clin Invest* **99**, 2165-2172.

Salmi M. and Jalkanen S. (2001). VAP-1: an adhesin and an enzyme. *Trends Immunol* **22**, 211-216.

Salmi M., Yegutkin G.G., Lehvonen R., Koskinen K., Salminen T., Jalkanen S. (2001b). A cell surface amine oxidase directly controls lymphocyte migration. *Immunity* **14**, 265-276.

Salmi M, and Jalkanen S. (2011). Homing-associated molecules CD73 and VAP-1 as targets to prevent harmful inflammations and cancer spread. *FEBS Lett* **585**, 1543-1550.

Salter-Cid L.M., Wang E., O'Rourke A.M., Miller A., Gao H., Huang L., Garcia A., Linnik M.D. (2005). Anti-inflammatory effects of inhibiting the amine oxidase activity of semicarbazide-sensitive amine oxidase. *J Pharmacol Exp Ther* **315**, 553-562.

Sans M., Fuster D., Vázquez A., Setoain F.J., Piera C., Piqué J.M., Panés J. (2001). ^{123}Iodine-labelled anti-VCAM-1 antibody scintigraphy in the assessment of experimental colitis. *Eur J Gastroenterol Hepatol* **13**, 31-38.

Serhan C.N. and Savill J. (2005). Resolution of inflammation: the beginning programs the end. *Nat Immunol* **6**, 1191-1197.

Smith D.J., Salmi M., Bono P., Hellman J., Leu T., Jalkanen S. (1998). Cloning of vascular adhesion protein 1 reveals a novel multifunctional adhesion molecule. *J Exp Med* **188**, 17-27.

Solé M., Hernandez-Guillamon M., Boada M., Unzeta M. (2008). p53 phosphorylation is involved in vascular cell death induced by the catalytic activity of membrane-bound SSAO/VAP-1. *Biochim Biophys Acta* **1783**, 1085-1094.

Springer TA. (1994). Traffic signals for lymphocyte recirculation and leukocyte emigration: the multistep paradigm. *Cell* **76**, 301-314.

Stephenson T. J. (2004). Inflammation. In a book: *General and systematic pathology*, edited by Underwood J. C. E. Elsevier, London pp 202-220.

Stolen C.M., Yegutkin G.G., Kurkijärvi R., Bono P., Alitalo K., Jalkanen S. (2004). Origins of serum semicarbazide-sensitive amine oxidase. *Circ Res* **95**, 50-57.

Stolen C.M., Marttila-Ichihara F., Koskinen K., Yegutkin G.G., Turja R., Bono P., Skurnik M., Hänninen A., Jalkanen S., Salmi M. (2005). Absence

of the endothelial oxidase AOC3 leads to abnormal leukocyte traffic in vivo. *Immunity* **22**, 105-115.

Teräs M., Tolvanen T., Johansson J.J., Williams J.J., Knuuti J. (2007) Performance of the new generation of whole-body PET/**CT** scanners: Discovery STE and Discovery VCT. *Eur J Nucl Med Mol Imaging* **34**,1683-1692.

Tohka S., Laukkanen M., Jalkanen S., Salmi M. (2001). Vascular adhesion protein 1 (VAP-1) functions as a molecular brake during granulocyte rolling and mediates recruitment in vivo. *FASEB J* **15**, 373-382.

Tran L., Vogel W.V., Sinaasappel M., Muller S., Baars J.W., van Rijswijk M., Dinant H.J., Beijnen J.H., Huitema A.D. (2011). The pharmacokinetics of ^{124}I-rituximab in patients with rheumatoid arthritis. *Hum Antibodies* **20**, 7–14.

Ujula T., Salomäki S., Virsu P., Lankinen P., Mäkinen T.J., Autio A., Yegutkin G.G., Knuuti J., Jalkanen S., Roivainen A. (2009). Synthesis, ^{68}Ga labeling and preliminary evaluation of DOTA peptide binding vascular adhesion protein-1: a potential PET imaging agent for diagnosing osteomyelitis. *Nucl Med Biol* **36**, 631-641.

Vainio P.J., Kortekangas-Savolainen O., Mikkola J.H., Jaakkola K., Kalimo K., Jalkanen S., Veromaa T. (2005). Safety of blocking vascular adhesion protein-1 in patients with contact dermatitis. *Basic Clin Pharmacol Toxicol* **96**, 429-435.

Visser E.P., Disselhorst J.A., Brom M., Laverman P., Gotthardt M., Oyen W.J., Boerman O.C. (2009) Spatial resolution and sensitivity of the Inveon small-animal PET scanner. *J Nucl Med* **50**, 139-147.

Vos F.J., Bleeker-Rovers C.P., Corstens F.H., Kullberg B.J., Oyen W.J. (2006). FDG-PET for imaging of non-osseous infection and inflammation. *Q J Nucl Med Mol Imaging* **50,** 121-130.

Weiner R.E., Sasso D.E., Gionfriddo M.A., Syrbu S.I., Smilowitz H.M., Vento J., Thrall R.S. (1998). Early detection of bleomycin-induced lung injury in rat using indium-111-labeled antibody directed against intercellular adhesion molecule-1. *J Nucl Med* **39**, 723-728.

Wen X., Wu Q., Ke S., Ellis L., Charnsangavej C., Delpassand A.S., Wallace S., Li C. (2001). Conjugation with (111)In-DTPA-poly(ethylene glycol) improves imaging of anti-EGF receptor antibody C225. *J Nucl Med* **42**, 1530-1537.

Wilson C.B., Snook D.E., Dhokia B., Taylor C.V., Watson I.A., Lammertsma A.A, Lambrecht R., Waxman J., Jones T., Epenetos A.A. (1991). Quantitative measurement of monoclonal antibody distribution and blood flow using positron emission tomography and ^{124}iodine in patients with breast cancer. *Int J Cancer* **47**, 344–347.

Wu AM. (2009). Antibodies and antimatter: the resurgence of immuno-PET. *J Nucl Med* **50**, 2-5.

Wu Y., Zhang X., Xiong Z., Cheng Z., Fisher D.R., Liu S., Gambhir S.S., Chen X. (2005). microPET imaging of glioma integrin {alpha}v{beta}3 expression using (64)Cu-labeled tetrameric RGD peptide. *J Nucl Med* **46**, 1707-1718.

Wu Z., Li Z.B., Cai W., He L., Chin F.T., Li F., Chen X. (2007). ^{18}F-labeled mini-PEG spacered RGD dimer (^{18}F-FPRGD2): synthesis and microPET imaging of $\alpha_v\beta_3$ integrin expression. *Eur J Nucl Med Mol Imaging* **34**, 1823-1831.

Xu H.L., Salter-Cid L., Linnik M.D., Wang E.Y., Paisansathan C., Pelligrino D.A. (2006). Vascular adhesion protein-1 plays an important role in postischemic inflammation and neuropathology in diabetic, estrogen-treated ovariectomized female rats subjected to transient forebrain ischemia. *J Pharmacol Exp Ther* **317**, 19-29.

Yamada S., Kubota K., Kubota R., Ido T., Tamahashi N. (1995). High accumulation of fluorine-18-fluorodeoxyglucose in turpentine-induced inflammatory tissue. *J Nucl Med* **36**, 1301-1306.

Yegutkin G.G., Salminen T., Koskinen K., Kurtis C., McPherson M.J., Jalkanen S., Salmi M. (2004). A peptide inhibitor of vascular adhesion protein-1 (VAP-1) blocks leukocyte-endothelium interactions under shear stress. *Eur J Immunol* **34**, 2276-2285.

Yoong K.F., McNab G., Hübscher S.G., Adams D.H. (1998). Vascular adhesion protein-1 and ICAM-1 support the adhesion of tumor-infiltrating lymphocytes to tumor endothelium in human hepatocellular carcinoma. *J Immunol* **160**, 3978-3988.

Zalutsky M.R. (2006). Potential of immuno-positron emission tomography for tumor imaging and immunotherapy planning. *Clin Cancer Res* **12**, 1958-1960.

Zhang X., Xiong Z., Wu Y., Cai W., Tseng J.R., Gambhir S.S., Chen X. (2006). Quantitative PET imaging of tumor integrin alphavbeta3 expression with ^{18}F-FRGD2. *J Nucl Med* **47**, 113-121.

Zinn K.R., Chaudhuri T.R., Smyth C.A., Wu Q., Liu H.G., Fleck M., Mountz J.D., Mountz J.M. (1999). Specific targeting of activated endothelium in rat adjuvant arthritis with a ^{99m}Tc-radiolabeled E-selectin-binding peptide. *Arthritis Rheum* **42**, 641-649.

Zorzano A., Abella A., Marti .L, Carpéné C., Palacín M., Testar X. (2003). Semicarbazide-sensitive amine oxidase activity exerts insulin-like effects on glucose metabolism and insulin-signaling pathways in adipose cells. *Biochim Biophys Acta* **1647**, 3-9.